LOW-TEMPERATURE SPECIFIC HEATS OF FACE-CENTERED CUBIC RUTHENIUM-RHODIUM AND RHODIUM-PALLADIUM ALLOYS

Thesis for the Degree of Ph. D.

MICHIGAN STATE UNIVERSITY

PAUL JA-MIN TSANG

1968

This is to certify that the

thesis entitled

LOW-TEMPERATURE SPECIFIC HEATS OF FACE-CENTERED CUBIC Ru-Rh and Rh-Pd ALLOYS

presented by

Paul Ja-Min Tsang

has been accepted towards fulfillment
of the requirements for

Ph.D. degree in Metallurgy

Chuan Tung Wei
Major professor

Date April 4, 1968

O-169

ABSTRACT

LOW-TEMPERATURE SPECIFIC HEATS OF FACE-CENTERED CUBIC RUTHENIUM-RHODIUM AND RHODIUM-PALLADIUM ALLOYS

by Paul J. M. Tsang

The specific heats of a number of face-centered cubic ruthenium-rhodium and rhodium-palladium alloys were determined between 1.4° and 4.2°K. Taking the Fermi level of palladium as a reference, the density of states, N(E), was deduced from the electronic specific heat coefficient γ of each of the alloys, and was plotted against the energy E. The N(E) versus E curve thus constructed shows features in qualitative agreement with the total density-of-states curve calculated for the 3d bands in face-centered cubic nickel by G. F. Koster, and that for the 4d bands in face-centered cubic palladium by P. Lenglart et al. as well, both of the calculations using the approximate method of Linear Combination of Atomic Orbitals, the L.C.A.O. method. The present results indicate that for the same face-centered cubic structure the general features of the 4d bands in the second-long-period transition metals are similar to those of the 3d bands in the first-long-period transition metals, and that the L.C.A.O. method for treating the d-electrons in the transition metals is essentially correct.

LOW-TEMPERATURE SPECIFIC HEATS OF FACE-CENTERED CUBIC RUTHENIUM-RHODIUM AND RHODIUM-PALLADIUM ALLOYS

By

Paul Ja-Min Tsang

A THESIS

Submitted to
Michigan State University
in partial fulfillment of the requirements
for the degree of

DOCTOR OF PHILOSOPHY

Department of
Metallurgy, Mechanics and Materials Science

1968

ACKNOWLEDGMENTS

My sincere gratitude is due to Professor C. T. Wei, for his patient guidance and advice. I am indebted to my colleague Mr. A. V. S. Satya for his assistance in many experimental works and to Dr. C. H. Cheng of Dow Chemical Company, Midland, Michigan for lending me drawings of an arc furnace used in this investigation. Acknowledgments are also due to Mr. J. W. Hoffman and Mrs. Barbara Judge of the Division of Engineering Research, College of Engineering for their cooperative assistance. Finally, I wish to express my thanks to National Science Foundation for the financial support of this investigation.

TABLE OF CONTENTS

LIST OF TABLES

LIST OF FIGURES

CHAPTER I

INTRODUCTION

Owing to the complexity of the physical and chemical properties of the transition metals, divergent theories have been proposed for the electronic structures of the transition metals since Slater and Stoner's initiation of the search [1, 2]. Among them four major models stand out, namely, Slater and Stoner's band or itinerant electron model, Pauling's valence bond model [3], Van Vleck's minimum polarity model [4], and Mott and Steven's s-d model [5]. In Slater and Stoner's band model, the d-electrons are regarded as being itinerant and describable by Bloch functions. Energy bands form due to the perturbation of the lattice potential. Such properties of the transition metals as the conduction by d-electrons, a large low-temperature electronic specific heat, and a high cohesive energy, can all be explained well by this model. However, in its earlier form, the theory is not adequate in interpreting the occurrence of ferromagnetism in Fe, Co, and Ni. Pauling's valence bond model is an extreme example of localized d-electrons. In this model a d-electron of one atom joins with a d-electron of a neighboring atom forming a singlet state. They are thus not coupled to other electrons

of their own atoms. By assigning proper spins of the d-electrons, Pauling was able to explain the saturation magnetic moments of Fe, Co, and Ni in an empirical way. However, except the cohesive energy, Pauling's theory does not explain the other important properties of the transition metals.

The essence of Van Vleck's minimum polarity model is the forming of a total energy level by the hybridization of the various states localized at the individual atoms. For example, if the ground state of a free atom of a particular transition element is $3d^8 4s^2$, the total ground state of this element in the metallic state would be a mixture of $3d^{10}$, $3d^9$, and $3d^8$ atomic states. This model is essentially a way of putting a correlation into the itinerant description of the d-electron; the energy band is formed by the inter-atomic exchange of the atomic states.

The s-d model was first proposed by Mott and Stevens, and was modified by Lomer and Marshall [6]. There are three main features in this model: (a) The ns-electrons in the outermost orbit of a metal atom are free, part of the (n-1) d-electrons are free and part of them are bound. The itinerant d-electrons belong to t_{2g} symmetry, while the bound ones belong to E_g symmetry. (b) If an integral occupation occurs, the E_g electrons will carry most of the magnetic moment of the metal. (c) The exchange coupling between the itinerant s-electrons and the bound d-electrons gives

rise to a non-integral magnetic moment of the metal. This exchange coupling is also ascribed as being the cause of the large cohesive energy of the transition metals.

In spite of the discrepencies between the above models, the band or itinerant picture enters into each of these models in one way or another [7]. Several approximation models have been used to calculate the energy band of the transition metals. Krutter [10] and Slater [2] first used the cellular method to calculate the combined s-d band of Cu. A narrow d-band with a high density of states was found to overlap with a broad s-band. Since the high speed computer became available, the augmented-plane-wave (APW) method [8], originated from the cellular method, has been proved to be one of the most powerful tools for solving the energy-band problems of solids. The APW method was first proposed by Slater [11] in 1937 and modified later by Saffren and Slater [12, 13]. Using the APW method, the energy bands of most of the first long period transition metals have been calculated by various investigators: the energy band of Cu by Burdick [14], that of bcc Fe by Manning [15], fcc Fe by Green [16], and Ni by Hanus [17]. Louks [18], using the APW method, calculated the Fermi surfaces of Cr, Mo, and W. In order to see the general trend of the energy band changing from one element to the next in the iron series metals, namely, the elements Ar, Co, Ni, Cu, V, Cr, Fe, Ti, and Zn, Mattheiss [19] used the APW method to calculate the energy bands of these metals along a particular

direction in the first Brillouin zone. He found that a rigid band model could be applied to alloys of the transition metals. The energy bands of bcc and fcc iron were recalculated by Wood [20]. The density-of-states curve obtained by Wood agrees qualitatively with that deduced by Wei, Cheng, and Beck [21] from their low-temperature electronic specific-heat data.

Fletcher first used the tight-binding (T-B) method to calculate the 3d band in Ni. The method was simplified by Slater and Koster in 1954 [24]. Since then it has been used extensively for calculating the d-bands of the transition metals. The band structures of cubic transition metals were calculated by Slater and Koster [24, 25] using their simplified T-B method. Belding [26] modified the calculation by introducing the interaction between next nearest neighbors and found a broadening in the lower part of the energy band for the bcc structure. The energy band for the fcc structure remained unchanged in Belding's result. Other transition metals, the energy bands of which have been calculated by using the T-B method, are Cr by Asdente and Friedel [27], bcc Fe by Abate and Asdente [28], and Ni by Yamashita et al.[29]. The Fermi surfaces and the density-of-states curves of Pt and Pd were calculated by Friedel et al. [30, 31], taking into consideration the effect of the spin-orbital coupling.

Regardless of the approximation methods used in the calculations, the resulting d bands show some common features.

The five d wave functions of a free atom have two types of symmetry. Three of the five have the yx, xz, and zy type of symmetry, the other two have the x^2-y^2 and y^2-z^2 type. In both the bcc and fcc transition metals the crystal field causes the five d wave functions to split into two levels at the origin of the k-space, the two x^2-y^2 type wave functions become the higher energy states, the Γ_{12} states, and the three xy type wave functions become the lower, $\Gamma_{25'}$. The degeneracies of these states will be removed totally or partially as k moves away from the origin. Due to the perturbations of the periodic lattice potential, the electron energy states form five overlapping sub-d-bands crossing each other in the middle of the first Brillouin zone leaving degeneracies at certain points in the k-space. As shown in Fig. 1-1, along certain directions in the first zone partial or total hybridization between these sub-levels occurs. When total hybridization occurs, a pattern of energy levels shown in Fig. 1-2 will result. The two lowest bands will be made of bonding functions with the xy symmetry at the center of the zone, and of bonding functions with the x^2-y^2 symmetry at the boundary. The two highest bands will be made of antibonding x^2-y^2 functions at the center, and of antibonding xy functions at the boundary. The remaining band will be of bonding type with the xy symmetry at the center of the zone, and of the antibonding type functions with the xy symmetry at the boundary. This band will be broader than the others. The extent of this broadening depends upon the

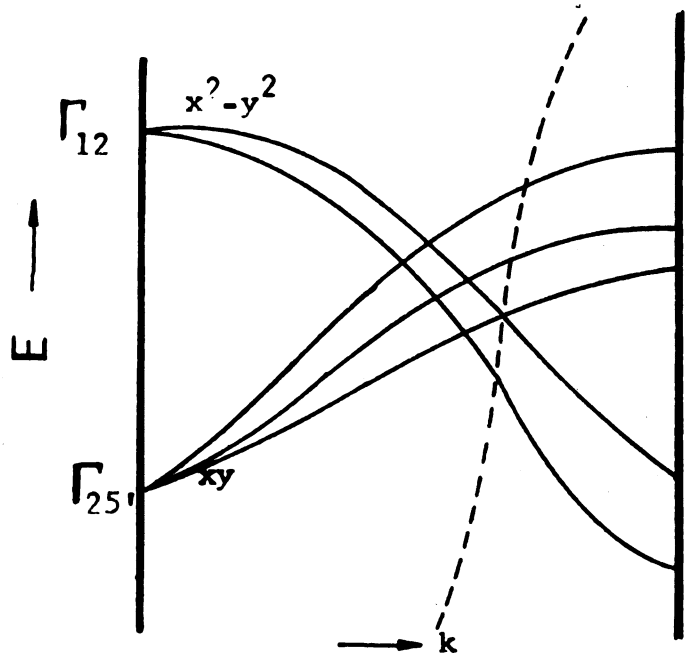

Fig. 1-1.--Degeneracies in k-space due to the perturbations of the periodic lattice potential.

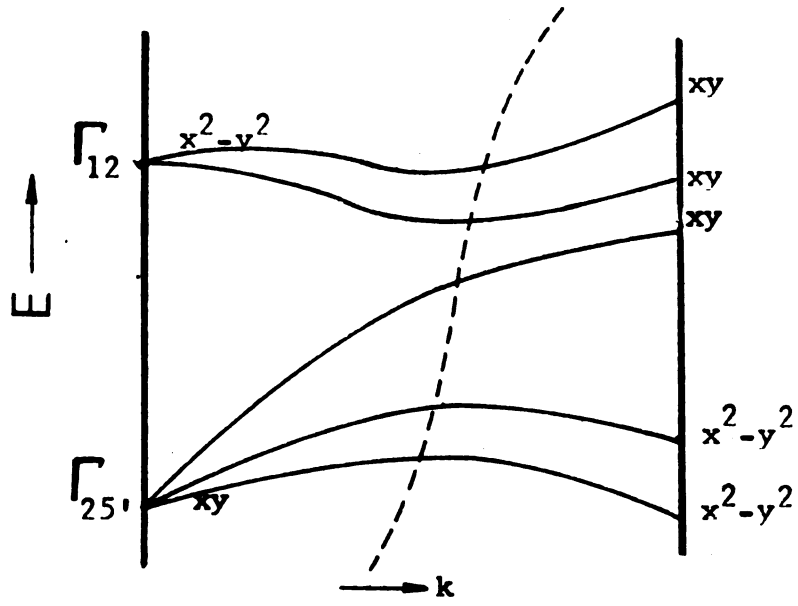

Fig. 1-2.--A pattern of energy levels when total hybridization occurs.

separation ΔE of Γ_{12} and $\Gamma_{25'}$. The density-of-states curve deduced from this general picture would thus be expected to have a minimum or a "valley" in the middle of the band [32]. Figure 1-3 shows the density-of-states curves for the five 3d sub-bands of Cr calculated by Asdente and Friedel [27]. This feature of having a "valley" in the middle of the d-band is prominent in the bcc transition metals calculated by using the APW or the tight-binding method. For the fcc metals, although this "valley" is still clearly seen in the d-band calculated by using the T-B method [25], it is, however, not clearly shown in that obtained by using the APW method [14, 26]. A new interpolation scheme for treating the electron energy bands particularly in the transition metals was proposed recently by Hodges et al. [33], and Mueller [34]. They treat the s-p conduction electrons with the pseudo-potential method and the d-electrons with the tight-binding method separately, and used the proposed interpolation scheme to obtain a hybridized total energy band. Except for a broadened "tail," the features of the hybridized energy band obtained by them for either the bcc Mn or fcc Cu are similar to those obtained by using the APW or T-B method.

There are several experimental methods that have been employed successfully in determining the Fermi surface of high purity metals, such as de Hass-van Alphen method, high field magnetoresistance method, Knight shift [54], and

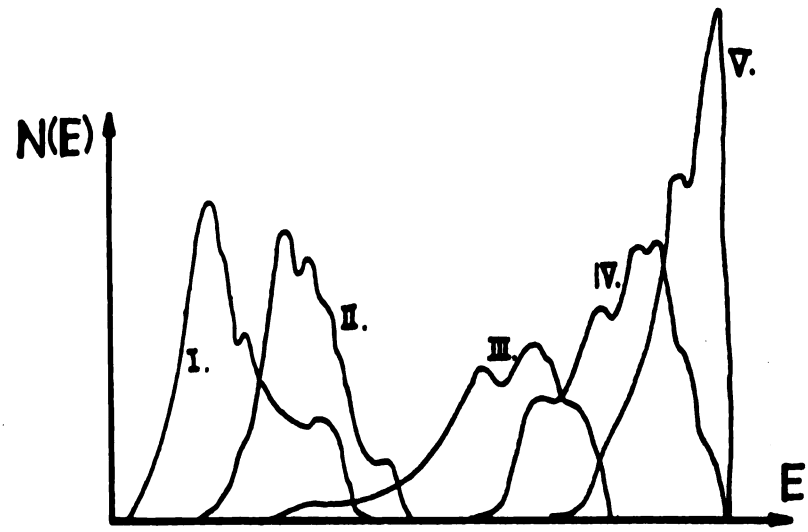

Fig. 1-3.--Energy band for 3d Cr. (Asdente et al.[27]).

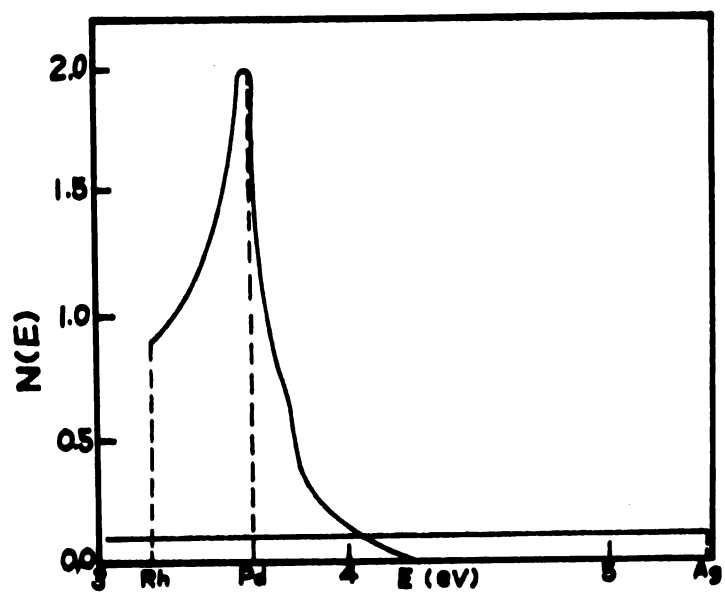

Fig. 1-4.--Upper part of 4d-band deduced from γ values of Rh-Pd and Pd-Ag alloys (Hoare [53]).

ultrasonic attenuation method [35]. For studying the structure of the electron energy band in metals the soft X-ray technique and photoemission technique [36] are also used. However, owing to the effect of impurity scattering, these methods are not suitable for studying alloys.

The possibility of separating the total Hamiltonian of a crystal into independent lattice and electronic Hamiltonians by using Born and Openheimer's adiabatic approximation enables one to regard the total heat capacity of a crystal as being essentially a linear sum of the various contributions of respectively the electrons, phonons, magnons, nucleons, and the interaction effects between them. At elevated temperatures, as the lattice specific heat is the major contribution, the heat capacity of simple solids such as the metals obeys Dulong and Petit law, and has a more or less constant value of 3R. At temperatures below $\theta/50$, the total heat capacity of a metal or an alloy can in most cases be written as a sum of the lattice and the electronic heat capacities.

$$Cv = \beta T^3 + \gamma T \qquad (1\text{-}1)$$

The T^3 term in the above equation is, according to Debye theory [1], the lattice specific heat. The coefficient β is related to the Debye temperature θ by

$$\beta = \left(\frac{12\pi}{5}\right) R \left(\frac{1}{\theta}\right)^{1/3} \qquad (1\text{-}2)$$

where R is the gas constant. The term linear in T is the electronic specific heat. It was first derived by Sommerfeld [38] based on an energy-band concept, and was found that γ for a free electron gas should be

$$\gamma = \frac{2}{3}\pi^2 k^2 N(E_f) \qquad (1\text{-}3)$$

where $N(E_f)$ is the density of states at the Fermi surface at the absolute zero of temperature. The electronic specific heat of a metal with an arbitrary band shape has been studied by Stoner [39]. He found that due to the irregular shape of the band, an additional term dependent on T^3 should be included in the heat capacity. The coefficient γ becomes

$$\gamma = \frac{2}{3}\pi^2 k^2 N(E_f)\ \{1+6(kT)^2[\frac{C_4}{C_2}\frac{N''(E_f)}{N(E_f)} - C_2(\frac{N'(E_f)}{N(E_f)})^2 + \cdots\cdot]\} \qquad (1\text{-}4)$$

Where $N'(E_f) = [\frac{d}{dE}N(E)]_{E=E_f}$, $N''(E_f) = [\frac{d^2}{dE^2}N(E)]_{E=E_f}$, $C_2 = \pi^2/12$, and $C_4 = 7\pi^4/720$.

The above review suggests that if the energy band concept is applicable to metals and alloys the value of γ will be directly proportional to the density of states at the Fermi level of the corresponding energy band. The additional term in T^3 will be small unless $N'(E_f)$ and/or $N''(E_f)$ is very large. Thus the value of γ may give a reasonable estimate of

$N(E_f)$. Although the slope and the curvature of the density of states curve might affect the deduced Debye temperature, θ, their effect on γ and hence $N(E_f)$ will be small. This suggests the possibility of using the heat capacity measurement at low temperatures as a means for determining the electron-energy-band structure of metals and alloys in conjunction with a "rigid-band" model.

The rigid-band model implies that neither the shape nor the height of the energy band of a matrix metal would be changed by alloying, provided that the alloy is a solid solution, and that the crystal structure remains the same as that of the matrix metal. The only thing that would be affected by alloying is the number of conduction electrons and hence the position of Fermi level of the matrix metal. The addition of an alloy element with a valency higher than that of the matrix metal will add more electrons to the energy band of the matrix metal, and hence raise the Fermi level. On the other hand, the alloying of a matrix metal with an element of lower valence number will lower the Fermi level. However, the results of recent specific-heat measurements of alloys of the noble metals [41, 42, 40] seem to contradict this model. But theoretical band-structure calculations [43, 44] as well as some experimental results obtained with alloys of the transition metals [45] support the validity of the rigid band model in at least those alloys of neighboring transition elements in the periodic table.

Low temperature specific heats of binary bcc and fcc solid solution alloys of the first long period transition metals have been investigated by Wei, Cheng, Gupta and Beck [21, 45]. The N(E) versus E curve obtained by them agrees qualitatively with that obtained from the tight-binding calculation. As for the alloys of the second long period transition metals the magnetic susceptibilities and the heat capacities of Pd-Ag alloys and some Pd-Rh alloys have been measured by Hoare et al. [46, 47], and Montgomery et al. [48, 49]. Their results show that for the Pd-Ag alloys both the magnetic susceptibility and the electronic specific heat coefficient decrease with increasing silver content until the Ag content reaches 60 at.% and will then level off with small fluctuations. For the Rh-Pd alloys a peak is observed in both the χ versus e/a and γ versus e/a curves at an e/a of approximately 9.95, if the e/a for pure Pd is taken to be 10.0. A study of the Pd-H system [50] has also revealed that the leveling off of χ or γ at 55 at.% H. It may be concluded that there are about 0.55 holes per atom in the 4d-band of pure Pd. Lenglart et al. [31] have estimated the number of holes in their calculated 4d-band for Pd to be just 0.55 per atom. However, according to their measurement of the de Hass-van Alphen effect of Pd, Vuillemin and Priestley [51] reported that the number of holes in Pd should be 0.36 per atom. The results of Kimura et al.'s calculation [52] seem to support the last figure.

By using the rigid-band model, the upper part of the density-of-states curve of the 4d-band has been deduced by Hoare et al. [53] from their experimental γ values of Rh-Pd and Pd-Ag alloys, as shown in Fig. 1-4. As can be seen, the experimental curve is in qualitative agreement with that obtained theoretically by Burdick [14] for Cu and that by Lenglart et al. for Pd [31]. However, Hoare et al.'s work extends only to $Rh_{0.5}Pd_{0.5}$ of the Rh-Pd system, and the Ru-Rh system has not yet been investigated. Ru has a hexagonal close-packed structure at room temperature. It is expected that Ru would dissolve in fcc Rh to a large extent. The purpose of this work is to extend the investigation of the 4d-band of the second-long-period transition metals by measuring the low-temperature specific heats of fcc solid solution alloys of the Ru-Rh and Rh-Pd systems to the extent that such alloys could be found and which had not been investigated previously.

CHAPTER II

EXPERIMENTAL DETAILS

Alloy Preparation

An arc furnace for melting the alloys was constructed as shown in Fig. 2-1. It consists of three major parts: a furnace body, a water cooled crucible, and an electrode with a tungsten tip. The electrode is held in the furnace by a "cap assembly," which enables the electrode to swing through an angle of about 15 degrees. The electrode can be raised or lowered by turning the cap screw. The crucible can be rotated at a speed of 1.5 rpm. A ¼ HP motor drives the crucible.

The power source for the furnace is a Harnischfeger Model DCR-400-HFGW arc welder with a built-in r-f arc starter. The crucible is connected to the positive pole and is grounded, while the electrode is connected to the negative. In so doing, a stable arc can be obtained, and the possibility of contaminating the alloy by the metal ions which may come from the electrode is prevented.

The melting operation is first started by evacuating the furnace until the end pressure of the mechanical pump of about 10 μ is reached, followed by repeated flushing with an inert gas.

Legend of Figure 2-1.:

1 = Lower Chamber of the Furnace

2 = Lower Plate

3 = Pyrex Furnace Sleeve

4 = Upper Plate

5 = Ball Head

6 = Cap Screw Assembly

7 = Crucible

8 = Driving Pulley

9 = Tungsten Electrode Tip

10 = Water Cooled Electrode

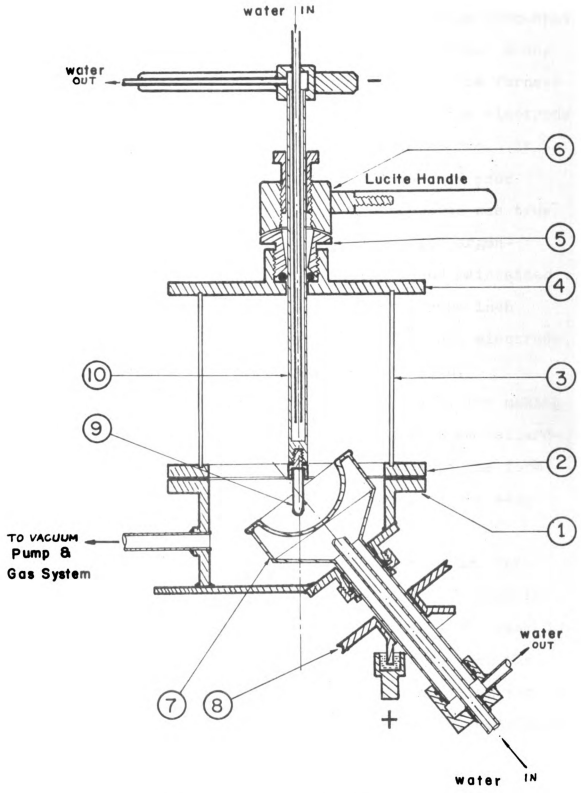

Fig. 2-1.--Arc Furnace.

It is not as easy to start an arc with a high frequency alternating current as with a direct contact method. Among the many controlling factors, the composition of the furnace atmosphere, and the distance between the tip of the electrode and the top of the charge are the most important two. It was found that the arc was easier to start but had poor stability in an argon atmosphere, and the opposite was true in a helium atmosphere. Thus, a 70:30 by volume argon-helium gas mixture was filled in the furnace and maintained at a positive pressure of about one lb. per square inch throughout the entire melting operation. The best electrode gap for the starting arc was found to be 1/8 inch.

The ruthenium, rhodium and palladium metals for making the alloys were 99.70% pure and were purchased from Gallard-Schlesinger Chemical Manufacturing Corporation in the form of rods. Their impurity contents as analysed by the same company are listed in Table II-1.

To make the alloys, the metal rods were broken into small pieces and were washed with hot diluted hydrochloric acid to eliminate any possible surface contamination caused by handling. The molten alloy can be made to roll in the crucible by slowly rotating the crucible and sweeping the arc over it. To ensure the homogeneity of the alloys, each alloy was melted at least three times. The alloys were weighed before and after the melting. The maximum loss of the metals due to evaporation in the entire alloy making process was less than

TABLE II-1.--Impurity content of Rh, Ru, and Pd metals.*

Impurity	Rh (%)	Ru (%)	Pd (%)
Ag	--	--	0.02
Al	0.001	0.001	0.003
Au	N.D.	N.D.**	0.001
B	--	--	0.001
Cu	0.001	0.005	0.01
Fe	0.01	0.01	0.05
Ir	0.02	N.D.	N.D.
Mg	0.0002	0.001	0.001
Mn	0.001	--	0.001
Mo	--	--	<0.001
Ni	--	--	0.005
Os	N.D.	X	N.D.
Pt	0.001	N.D.	0.02
Rh	Balance	0.003	0.003
Ru	N.D.	Balance	N.D.
Pd	0.005	0.005	Balance
Si	<0.001	--	0.1

*Analyzed spectrographically by Atomergic Chemetals Co., Garden City, L. I., N. Y.

**N.D. = element not detected; X = interference

0.5% for all the Ru-Rh alloys and less than 1.0% for the Pd-Rh alloys. Individual checks showed that the rates of loss for Ru and Rh were almost the same, while it was twice as much for Pd as for Rh.

The complete equilibrium diagram of neither Ru-Rh nor Pd-Rh has been reported. However, it is believed that there is a missibility gap in the middle portion of the Ru-Rh system. The Ru-rich side is a solid solution with an hcp structure, and has been explored by Hume-Rothery et al. [55a,b] whereas the Rh-rich solid solution has a fcc structure. The solubility limit of Ru in the fcc Rh-rich solid solution is believed to be approximately 40 at .% [56]. To confirm this, a series of test samples of various composition were made. The powder of each of the samples was encapsulated in a quartz tube and vacuum annealed at 1100°C for 24 hours and then water quenched. Debye-Scherrer X-ray patterns of the powder samples were then taken. The X-ray patterns confirm that up to 40 at .% Ru, the Ru-Rh alloys are fcc, single phase alloys, at least at high temperatures. Beyond that, two-phased alloys are formed. Palladium and rhodium are both fcc and completely intersoluble at high temperatures. Below 845°C, a concentrated alloy may separate into a phase mixture of Pd and Rh rich solid solutions [57]. However, this transition is very sluggish [58]. Alloys of a single fcc phase can be obtained by fast cooling through this temperature range.

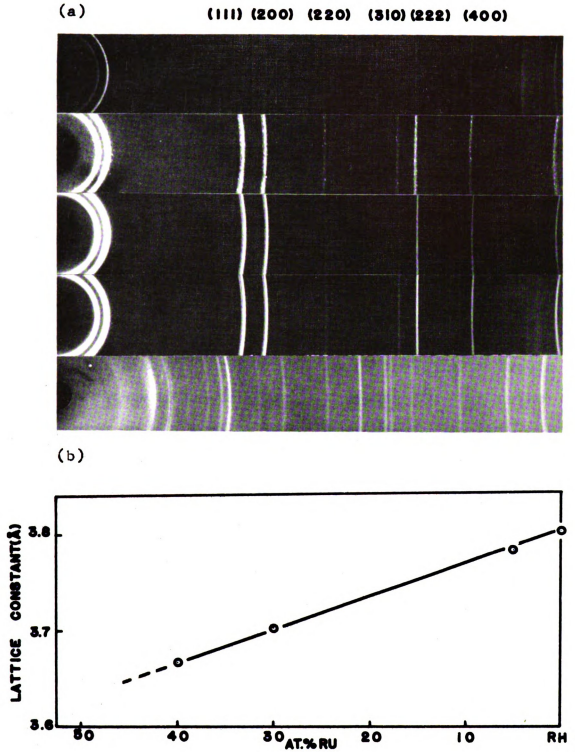

Fig. 2-2.--(a) Debye-Scherrer patterns of Rh & Ru-Rh alloys. From top to bottom are: pure Rh, 5at.% Ru-Rh, 30at.% Ru-Rh, 40at.% Ru-Rh, and 50at.% Ru-Rh. (b) Lattice constants of the Ru-Rh alloys as a function of Ru content in Rh.

Therefore, all the alloys used in this experiment were encapsulated in quartz tube, vacuum annealed at 1080°C for at least 24 hours, and then water quenched. Several samples were examined with an optical microscope, and no second phase was observed.

Cryogenic System

The main effort of this experiment was to measure adiabatically the temperature response of each alloy to an input of thermal energy at low temperatures. The equipment used for this experiment consisted of a cryogenic system to provide an adiabatic environment for the sample at liquid helium temperatures, and an electrical system to supply the thermal energy to the samples as well as to measure its response.

The entire set up of the cryogenic system was essentially the same as that used by C. T. Wei at the University of Illinois with only minor changes. The cryogenic system, consisting of a cryostat, a high vacuum pumping system, a low vacuum main pumping system, a manometer, and an inert gas system, is shown in Fig. 2-3. The construction of the cryostat is shown in Fig. 2-4. The details of the entire system may be referred to Wei's thesis [59]. Some modifications made on the cryostat system to suit this experiment and the capacity that can be achieved by the system are described in this section.

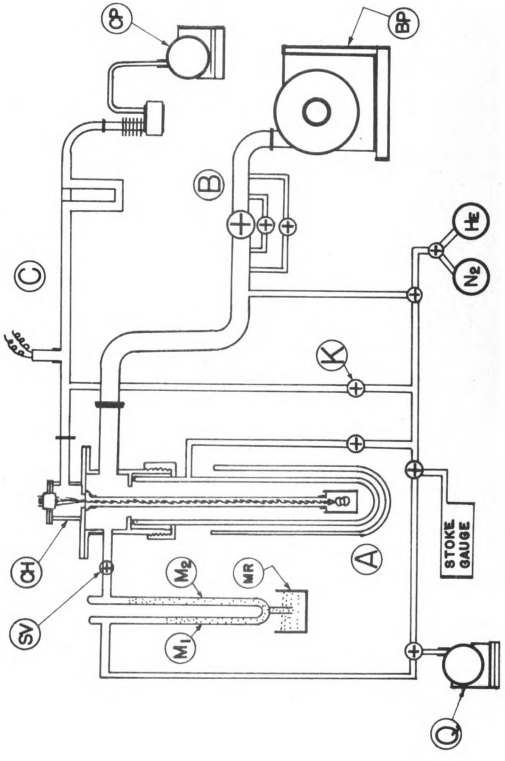

Fig. 2-3.--Cryogenic System.

Legend of Figure 2-4.:

A = Liquid Helium Feeding Hole

B = Connected to High Vacuum Pumping System

C = Calorimeter Can

D = Connected to Main Pumping System

H = Cryostat Head Assembly

K = Kovar Seal

P = Safety Valve

Q = Connected to Manometer

CH = Calorimeter Head Housing

Di = Inner Dewar

Do = Outer Dewar

S = Sample Assembly

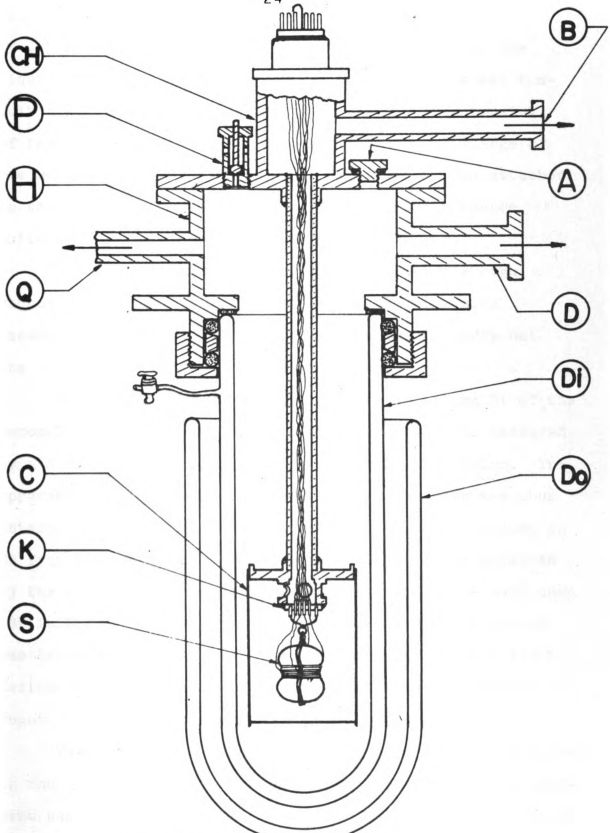

Fig. 2-4.--Cryostat System

The first modification was the elimination of the liquid nitrogen heat trap; instead, a stainless steel conduit connecting the calorimeter can and the head housing of the calorimeter was soldered directly to the flange of the head housing. In addition, a safety valve was attached to the flange so as to prevent any accidental pressure build-up inside the inner dewar.

Another modification was the insertion of a high vacuum stop valve between the manometer and the head assembly of the cryostat. This enables one to carry out the calibration of the thermometer alone.

As shown in Fig. 2-3, the pressure in column M1 of the manometer was kept at about 30μ by pump Q, and was measured by a Stoke's gauge during the thermometer calibration. The apparent vapor pressure of the liquid helium bath was thus obtained by subtracting the height of the mercury column in M2 from that in M1 plus the pressure in column M1 measured by the Stoke's gauge. The pumping capacity of the main pump (BP in Fig. 2-3) was about 1.6 cubic meter per minute; it was large enough to reduce the vapor pressure of the liquid helium bath to such an extent that a minimum temperature of about 1.25°K could be reached.

The highest vacuum that could be reached and maintained in the calorimeter by the high vacuum system in this experiment was 7.0×10^{-6} mm Hg, which was found to be sufficient for the experiment.

Sample Assembly

Owing to the difficulty of machining the alloys with ruthenium content higher than 20 at .%, alloy buttons in the shape obtained directly from melting were used to make the sample assembly. A heater-thermometer assembly matching the alloy buttons, was used for supplying the necessary thermal energy and to measure the change of temperatures of the sample during the experiment. The sample assembly, as shown in Fig. 2-5a, was made of two alloy buttons with a heater-thermometer assembly sandwiched in between. Fig. 2-5b shows the heater-thermometer assembly. A pure copper disk 1/2 inch in diameter and 1/8 inch thick was cut with a groove of 1/16 inch wide and 1/16 inch in depth around its circumference, and a 1/32 inch hole was drilled radially through its center. The copper disk served as the heater-thermometer body. No. 40 enamel-coated manganin wire with a nominal resistance of 31.4 ohm per foot was used for making the heater. It was wound around the circumferential groove of the copper disk in such a way that no net induced magnetic field would result from the heating current. The total resistance of the heater was approximately 300 ohm at room temperature. A 1/10 watt carbon resistor with a nominal resistance of 60 ohm at room temperature was used as the temperature sensing device and was placed in the radial hole at the center of the copper disk. As conducting leads, No. 38 double-cotton insulated copper wires of about 6 cm. long were connected to the ends of the heater and the

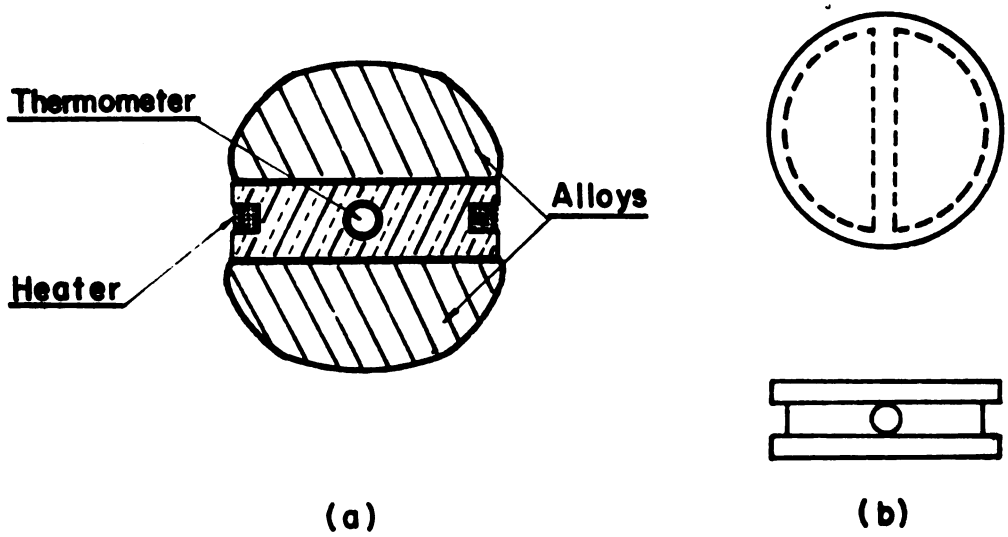

Fig. 2-5.--(a) Sample Assembly; (b) Heater-Thermometer Copper Body.

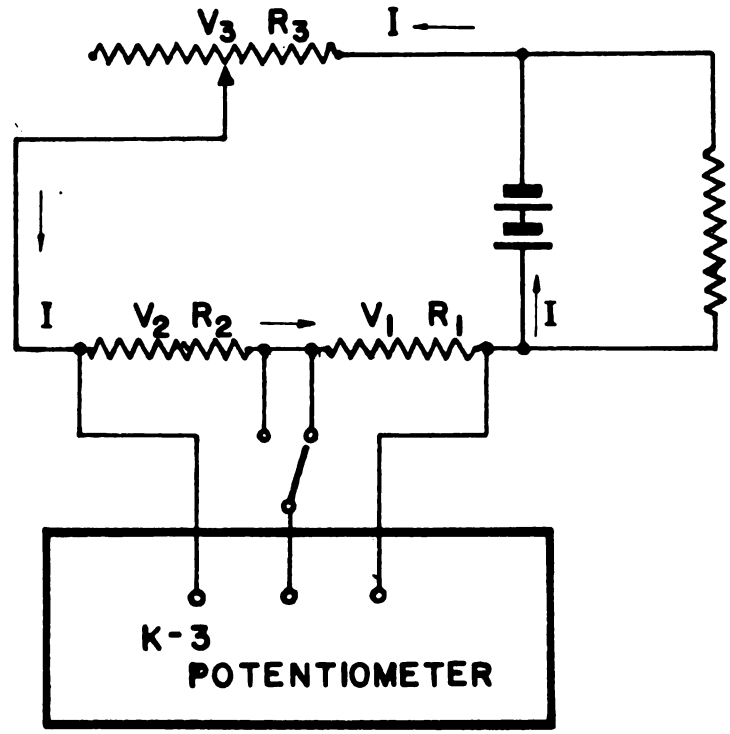

Fig. 2-6.--Essence of the Electrical Circuit.

carbon thermometer. The flat side of the heat-treated alloy buttons were ground and polished to a mirror finish. The surface of the heater-thermometer disk and the polished surface of the alloy buttons were coated with a thin layer of silicone grease before assembling. Alloy buttons and the heater-thermometer assembly were then tied together with thick copper wires to form the sample assembly.

The four electrical leads of the heater and the thermometer were connected to four corresponding measuring junctions on a kovar seal through short pieces of manganin wire. It was observed that the insertion of the manganin wires increased the thermal stability and decreased the temperature drifitng rate of the sample during the measurements.

Electrical Measurement

The essential purposes of the electrical circuit designed for this experiment were: first, to provide a certain amount of thermal energy to the alloy by sending a constant current through the heater for a certain period of time. This was the Joule heat of the heater, i.e.

$$E = i_h^2 \times R_h \times t$$

where E is the thermal energy input to the alloy in 10^{-6} joule, i_h is the heating current in milliampere, R_h is the resistance of the heater in ohm, and t is the time of heating period in seconds. Secondly, to record the temperature response of the

alloy to this thermal energy. In this experiment, this temperature response was measured as a resistance change in the carbon thermometer.

The principle used in measuring the resistance of the thermometer or the heating current can be illustrated in a simplified circuit as shown in Fig. 2-6. In Fig. 2-6, R_1 represents either the thermometer or the heater. R_2 is a standard resistor, and R_3 is a variable resistor. By varying R_3 a desired current I can be set up in the circuit. The current is measured by the voltage across the standard resistor R_2. R_1 can then be readily known by measuring the voltage drop V_1 across R_1. This can be done by using either a potentiometer or an electrometer.

Fig. 2-7 shows the circuit diagram for the electrical measurements. It is essentially the same as that used by Wei, et al. The main features of this circuit are: a Leeds-Northrup K-3 potentiometer with a d-c null detector for the standardization of the current I in both the thermometer and the heater circuits, and to measure the potential drop across the heater or the thermometer; a Speedomax recorder with a d-c amplifier for recording the continuous change in the resistance of the thermometer with time during a heating period; and a Berkeley Model 410 electronic counter coupled with a General Time 2001-2P type frequency standard for measuring the heating time. In addition, the on-off switch for the heater and that for the counter are synchronized through an electronic switch.

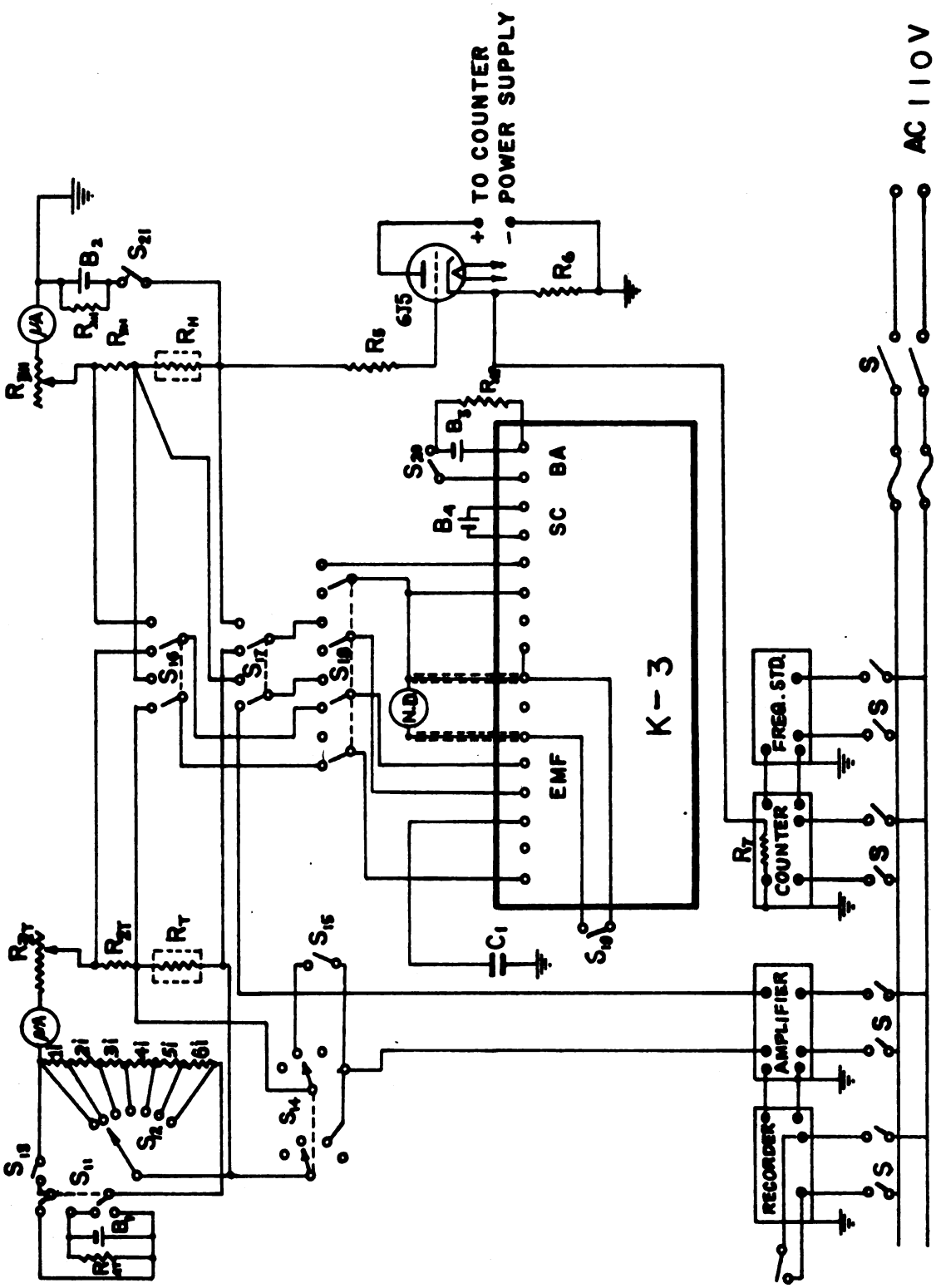

Fig. 2-7.--The Electrical Circuit.

The components of the electrical circuit are listed in Table II-2(a). The relative positions of the switches for the various functions are illustrated in Table II-2(b).

Experimental Procedures

There were four major steps in the low temperature specific heat measurements, namely:

1. Preparation of the calorimeter system and first stage cooling.
2. Standardization of the potentiometer as well as the heating and thermometer current.
3. Second stage cooling and the calibration of the thermometer against the vapor pressure of the liquid helium bath.
4. Heat capacity measurement.

The calorimeter system, after being set up, was first evacuated to an end pressure of about 2×10^{-5} mm. Hg. Any possible leakage was checked to make sure that the high vacuum can be sustained during the experiment. The system was then flushed with dry helium gas for several times. A small amount of helium gas (at a pressure of about 700 μ) was left and sealed in the calorimeter system for heat exchange. The inner dewar of the cryostat was also evacuated, flushed with dry helium gas, and filled with helium gas to a small positive pressure. For heat conduction, the jacket of the inner dewar was filled with nitrogen gas at a pressure of about 200 μ.

TABLE II-2(a).--Components of measuring circuit.

R(ohms)	B (Volts)	C (mfd)
1i 1.6 K 2i 4.7 K 3i 16 K 4i 16 K 5i 15 K 6i 18 K	B1 to B3; Butt-Sub Model BSTC-213 constant voltage supply 3 volts at 24.4 mA. B4 Cadmium Low Temperature Coefficient Standard Cell; 1.01925.	1 0.01
3T 0-1 Meg (General Radio Type 1432-M Decade Resistor; Minimum Scale 0-100 in ten steps)		
2T 10,000 Standard resistor T Thermometer (Varies from 800 at 4.2°K to 50,000 at 1.25°K)		
4T and 4H 2.2K		
3H 0-10 K (Decade Resistor; Minimum Scale 0-10 ohm in ten steps)		
2H 100 Standard Resistor H Heater (about 300)		
5 1 Meg.		
6 10 K		
4P 5 K		

TABLE II-2(b).--Positions of switches for various functions.

Function	Switches									
	12	13	14	15	16	17	18	19	20	21
Standardization of K-3 potentiometer	-	-	1	on	off	off	2	off	on	-
Standardization of Heating Current	off	-	1	on	2	off	1	off	on	on
Standardization of measuring current	on	adj	1	on	1	off	1	off	on	off
Measuring EMF of Heater	off	-	1	on	off	2	2	off	on	on
Measuring EMF of Thermometer	on	adj	2	on	off	1	2	off	on	off
Recording	on	adj	4	off	off	1	2	on	on	*
Calibration of D-C Amplifier & Recorder	off	-	3	off	off	1	2	on	on	off

*On for heating, off for stand-by.

This was checked before every experiment. Liquid nitrogen was then gradually filled into the outer dewar which had a permanent vacuum jacket. As the system was gradually cooled down, additional helium gas was gradually filled in the inner dewar to compensate for the contraction of the helium gas originally in it in order to maintain the positive pressure within the inner dewar. The maintaining of a positive pressure in the inner dewar was a necessary measure to prevent the leaking of air into the inner dewar when it was opened for filling of liquid helium. Five to seven hours were required to cool the system to the liquid nitrogen temperature. After the cryostat had been cooled down to the liquid nitrogen temperature, the electrical connections and any possible leakage of the calorimeter were again checked before the filling of liquid helium. The filling of liquid helium took less than five minutes to complete. Ten to fifteen minutes were usually needed for the sample assembly to reach a temperature equilibrium with the liquid helium bath.

The standardization of the K-3 potentiometer and the desired currents for the heater and the thermometer were carried out immediately after the sample assembly had reached the temperature equilibrium. A cadmium standard cell which had a low thermal coefficient served as the standard emf supply.

The calorimeter was further cooled down as the vapor pressure of the liquid helium in the inner dewar was gradually reduced by the main pumping system. In the mean time, the

R-T relationship of the thermometer was calibrated by measuring the vapor pressure of the liquid helium and the resistance of the thermometer simultaneously. The temperature of the liquid helium bath could be deduced from its vapor pressure using the NBS 1958 He^4 Scale of Temperature. The lowest temperature that could be reached in this experiment was 1.25°K. The resistance settings of the variable resistor R_{3_T} or R_{3_H} for the desired currents in the thermometer circuit or in the heater circuit respectively, as well as the resistance of the heater were all checked again at the lowest temperature for the stability of the instrumentation.

After the lowest temperature had been reached, the sample assembly was warmed up to about 1.4°K. The measurement of the heat capacity of the sample assembly was then carried out. The heater was turned on for a certain period of time while the temperature change of the sample assembly was automatically recorded by the Speedomax recorder. Fig. 2-8 shows three typical recorded curves. The ordinate of the figure represents the time while the abscissa is a measure of the temperature of the sample assembly. As shown in Fig. 2-8 curve (B), the initial temperature T_1 and the final temperature T_2 of the sample assembly are obtained by extrapolating the initial thermal drifting curve CA and the final thermal drifting curve BD to the mean time line. The difference between T_1 and T_2 is the temperature increment ΔT of the sample assembly corresponding to the thermal energy

input while their average is taken as the temperature to which the heat capacity of the sample assembly for the particular measurement pertains. Curve (A) in Fig. 2-8 with zero thermal drift before and after the heating is the ideal one. However, since it was impossible to achieve an absolute adiabatic environment, some thermal drifting in the sample would always be present. In order to obtain an acceptable accuracy, it was essential to manipulate the system so as to minimize the thermal drift and to have the tendencies of the drift before and after the heating in the same direction, as shown in curve (B) of Fig. 2-8. The most undesirable one is shown in Fig. 2-8 curve (C). In this case, the thermal drifts before and after the heating are large and in opposite directions. A large error may be introduced in evaluating T_1 and T_2.

The degree of vacuum in the calorimeter, methods of connecting the electrical leads to the measuring circuit, the way of suspending the sample assembly, and the degree of thermal equilibrium achieved in the sample assembly were all important factors governing the rate of the thermal drift. Among them, the degree of vacuum in the calorimeter was the most important one. It was found that a vacuum of lower than 5.0×10^{-5} mm Hg becomes undesirable. Usually the vacuum in the calorimeter was kept in the range of 8.0×10^{-6} mm Hg. to 1.4×10^{-5} mm Hg.

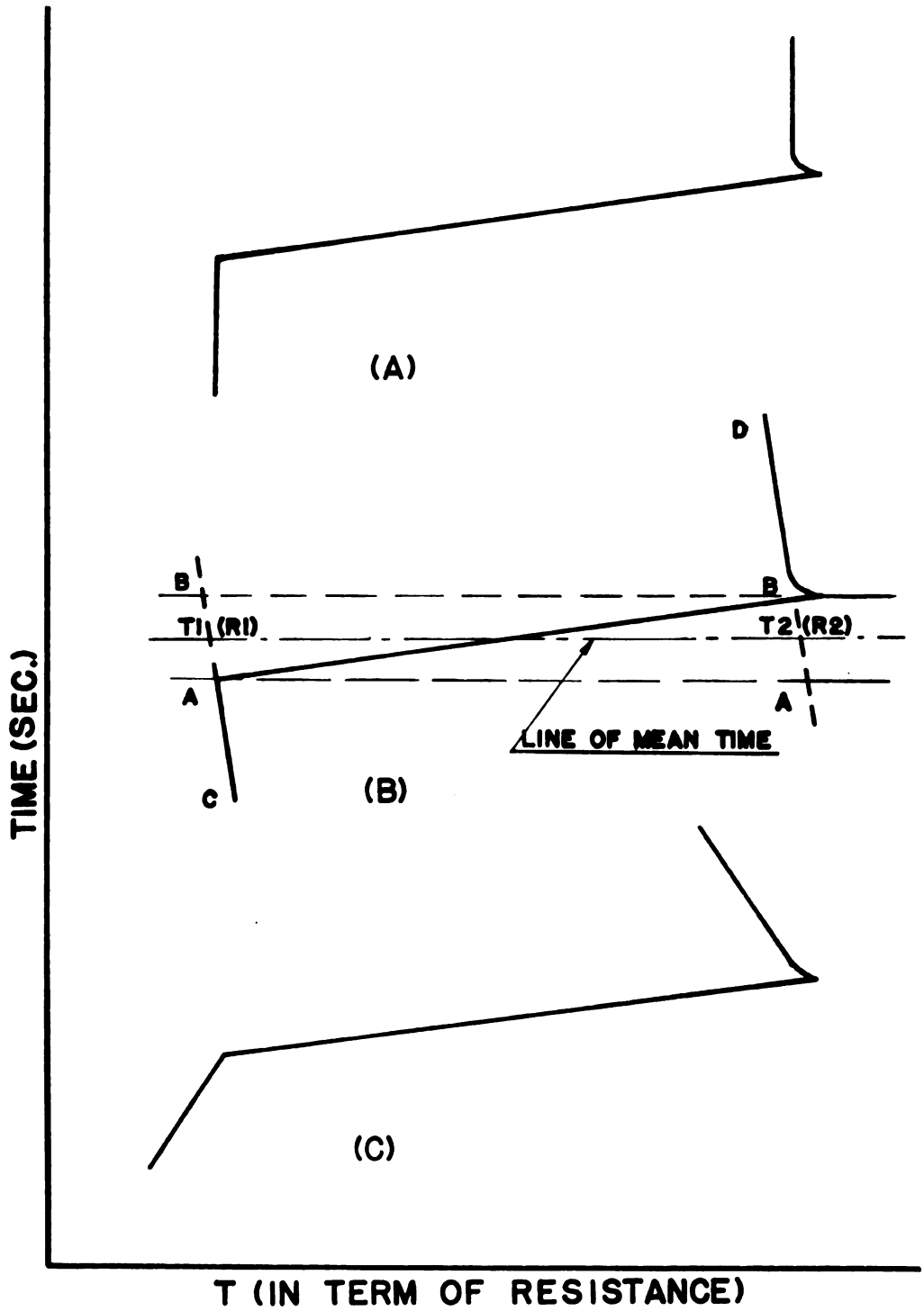

Fig. 2-8.--Experimental Time--Temperature Curves.

CHAPTER III

RESULTS AND CALCULATIONS

Calculations

According to Keesom and Pearlman [60], the characteristics of the carbon thermometer can be expressed in general as

$$(\ln R/T)^{\frac{1}{2}} = \sum_{i}^{N} A_i (\ln R)^i \qquad (3\text{-}1)$$

However, it has been found experimentally that only two terms of the polynomial are necessary to give enough accuracy [60].

$$(\ln R/T)^{\frac{1}{2}} = A + B \ln R \qquad (3\text{-}2)$$

In the temperature range of 1.6°K to 4.2°K a total number of 15 to 20 experimental points were usually taken during the calibration. Above the λ point, the vapor pressure of the liquid helium was corrected for the hydrostatic pressure due to its own head above the center of the calorimeter can. The resulting pressures were then converted to corresponding temperature values by using the 1958 He^4 Temperature Scale [61]. These and the corresponding resistances of the thermometer were then fitted with the equation (3-2) using a Control Data 3600 computer. The coefficients A and B of

(3-2) were obtained by using the least squares method. It was found in the early stage of this investigation that the accuracy of measuring the vapor pressure of liquid helium near its λ point is poor and a rather large error could thus be introduced. It was decided to avoid the neighborhood of the λ point in the calibration in the later experiments. In general, the maximum error in the calibration was ±0.15%. A typical calibration curve is shown in Fig. 3-1.

The thermal energy input into the sample assembly was shared by the alloy, the copper wire used for assembling, and the heater-thermometer assembly. In order to calculate the heat capacity of the alloy, it was therefore necessary to subtract the amount of heat energy absorbed by the copper wire and the heater-thermometer assembly from the total heat input.

As described in Chapter II, the heater-thermometer assembly was mainly composed of a pure copper disk, a small carbon resistor, about ten feet of number 40 manganin wire, four short pieces of number 40 double cotton-coated copper wire, and a small amount of vacuum grease. The total weight of the assembly amounted to 5.5 grams; out of this, more than five grams belonged to the pure copper disk. Therefore, it was reasonable to assume that the heat capacity of the heater-thermometer assembly was essentially the same as that of pure copper without introducing too much error. The heat capacity per mole of the heater-thermometer assembly and the tying copper wire combined is

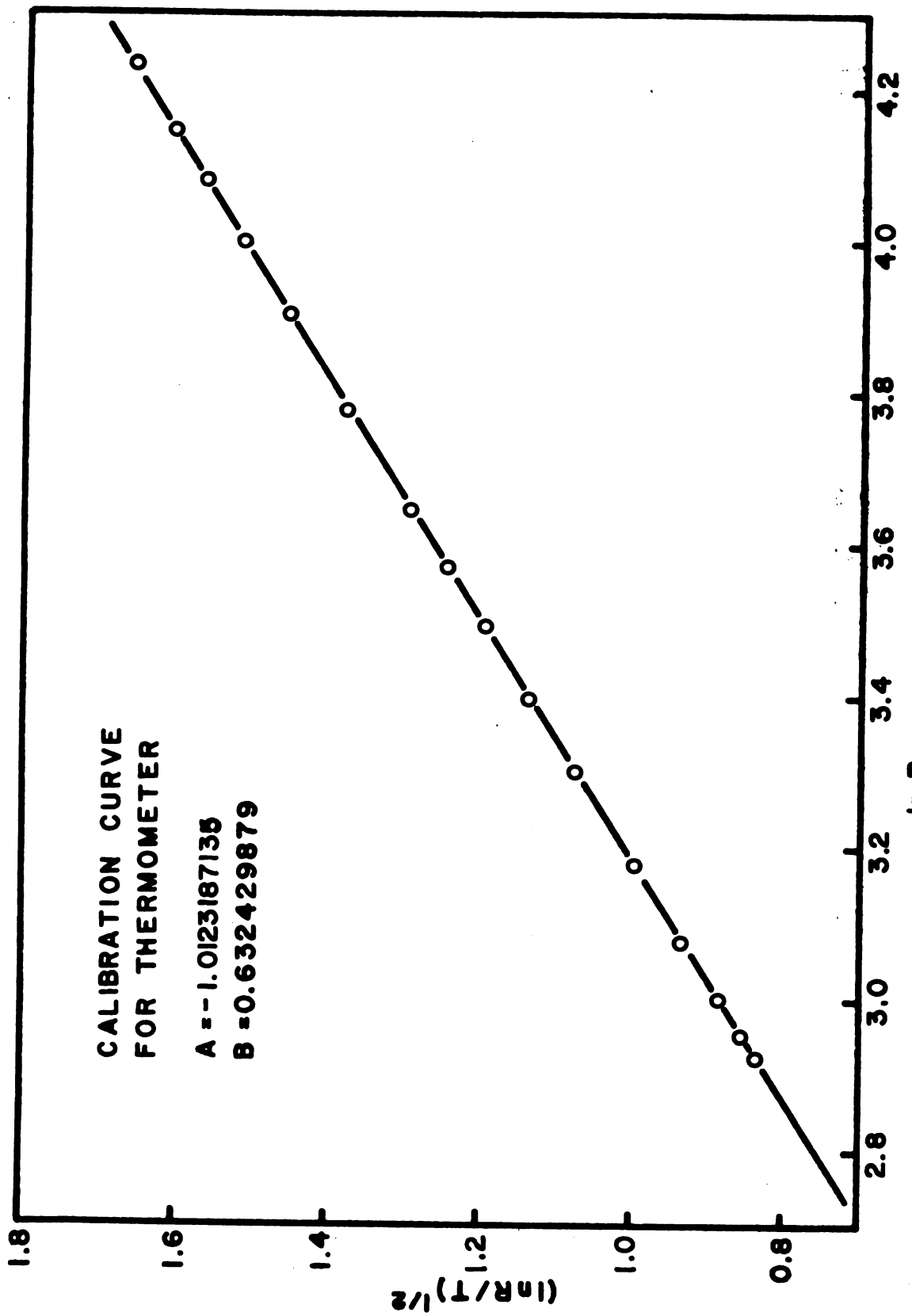

Fig. 3-1.--Calibration Curve for the Thermometer used in Sample PT-15.

$$C_{v,th} = \gamma T + (12/5)\pi^4 R_h (T/\theta)^3 \qquad (3\text{-}3)$$

where R_h is the gas constant and θ, the Debye temperature. Substituting $\gamma = 1.8 \times 10^{-4}$ cal./mole-deg^2 and $\theta = 315°K$ of pure Cu [62,63], equation (3-3) becomes

$$C_{v,th} = 1.8 \times 10^{-4} T + (1.815 \times 10^{-4}/14.5973) T^3 \qquad (3\text{-}4)$$

Therefore, the heat capacity of the alloy is

$$C_v = (i^2 Rt/K - C_{v,th} \times N_1)/\Delta T \times N_2 \qquad (3\text{-}5)$$

where

i = heating current in amperes

R = resistance of heater in ohms

t = time of heating period in seconds

N_1 = number of moles of the heater-thermometer assembly and the tying copper wires combined

ΔT = the increment of temperature of the sample assembly during each heating period

N_2 = number of moles of the alloy

K = conversion factor from Joules to calories = 4.184

A correction was further made in the thermal energy input for the heat dissipated in the inserted manganin wire.

Results

Altogether fourteen samples, including a pure Rh and a pure Pd, were measured. For each sample, a number of thirty two to fifty data points were taken, and their specific heat capacities were calculated according to Eq. (3-5). The C_v/T versus T^2 curves of the samples are shown in Figures 3-2 to 3-5, and their detailed experimental results are tabulated in Appendix A. As can be seen, some of the C_v/T versus T^2 curves have indeed good linearity whereas others show anomalous curving-up at the lower temperature part. These anomalies are obviously either due to experimental error or to some unknown causes. This will be elaborated further in the next chapter. However, to the first approximation, the experimental data of each sample were fitted to the heat capacity equation for metals and alloys at low temperatures

$$C_v/T = \gamma + \beta T^2 \qquad (3\text{-}6)$$

and by using the least squares method, the values of γ and β of the alloys were found by extrapolating the linear part of the C_v/T versus T^2 curves to zero temperature and ignoring the low temperature anomaly. From β the Debye temperature of each of the alloys was then calculated:

$$\theta = (12\pi^4/5)^{1/3}(R)^{1/3}(\beta)^{-1/3} \qquad (3\text{-}7)$$

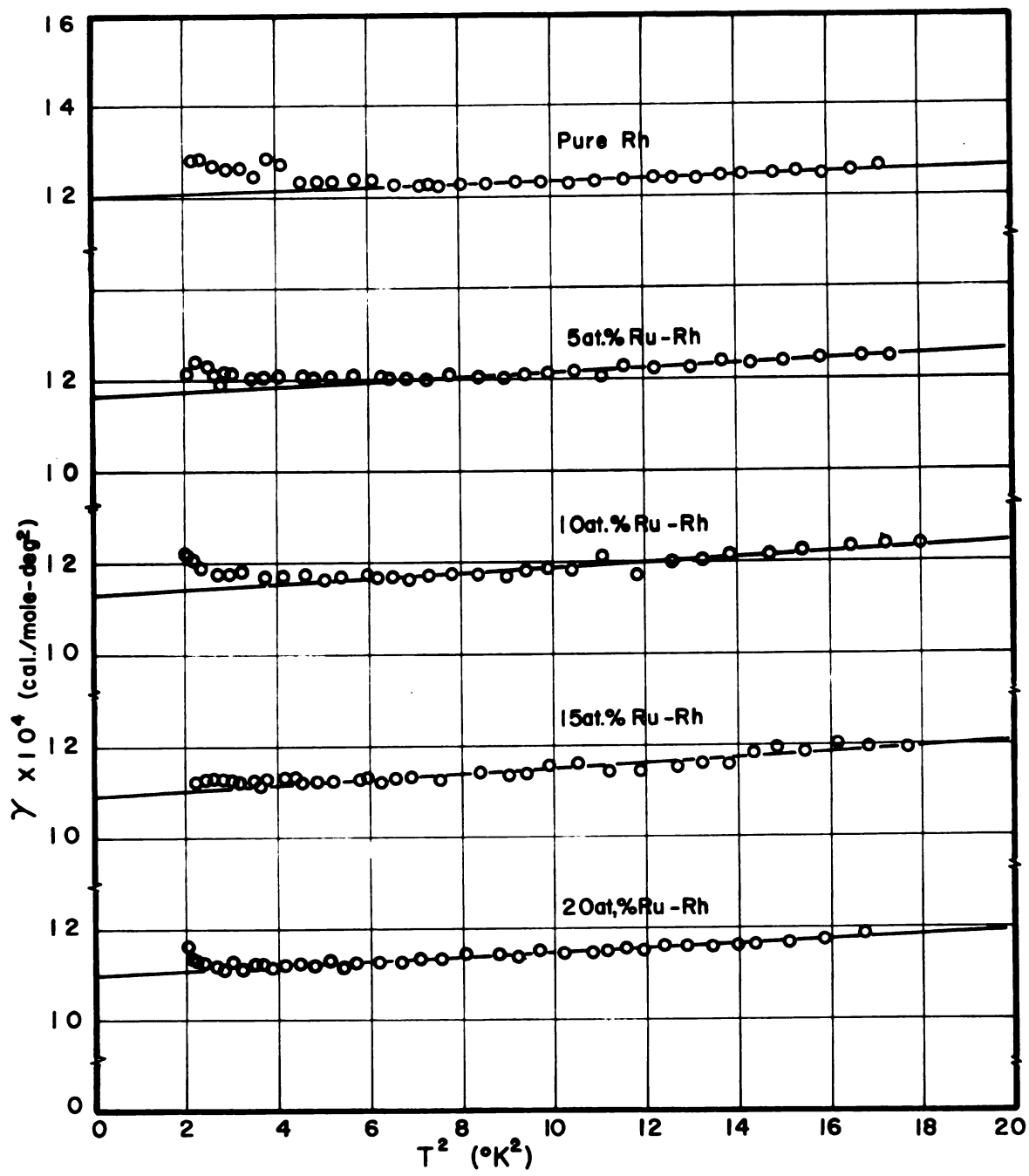

Fig. 3-2.--C_v/T vs T^2 Curves of Pure Rh and Ru-Rh Alloys.

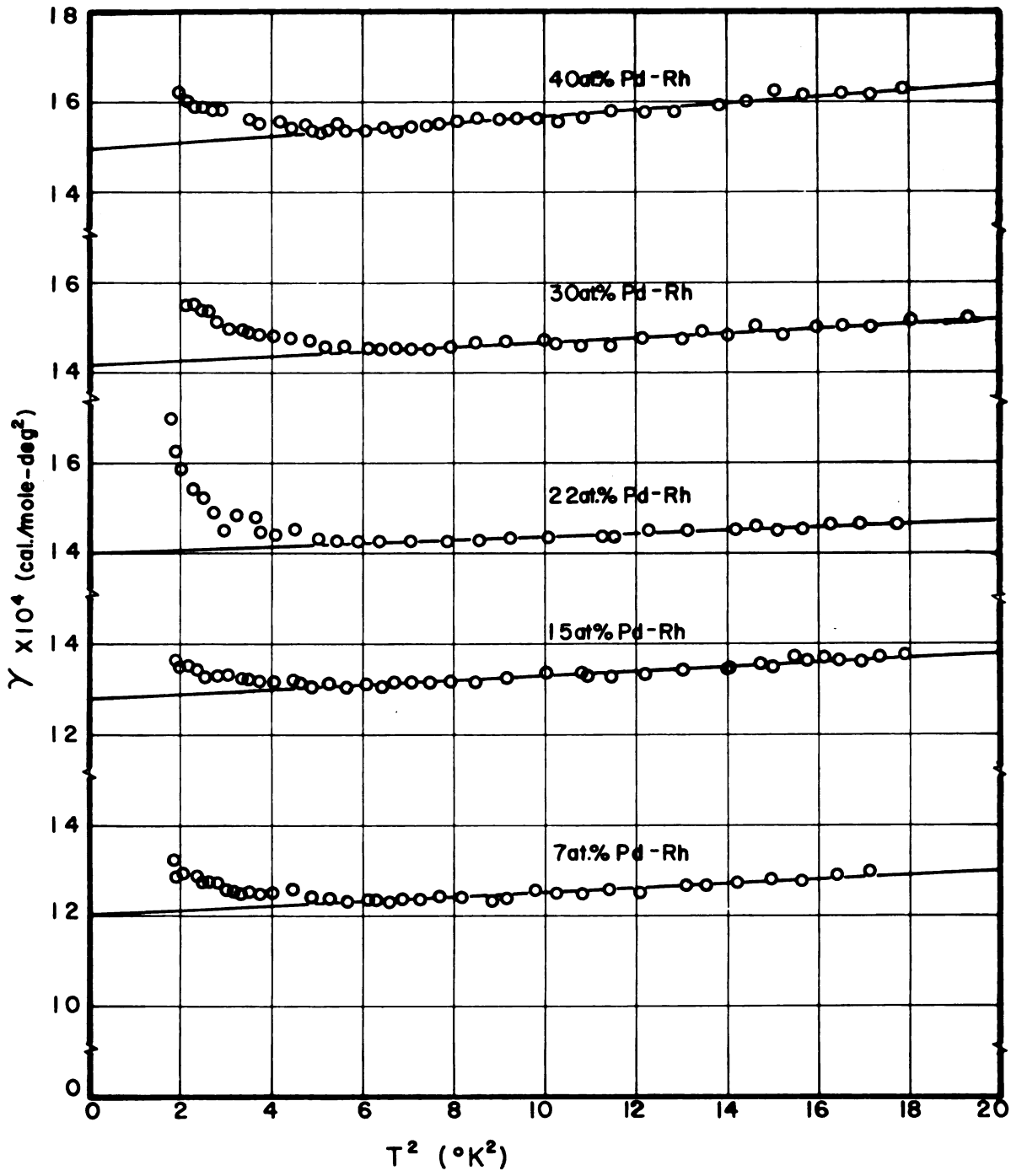

Fig. 3-3.--C_v/T vs T^2 Curves of Rh-Pd Alloys.

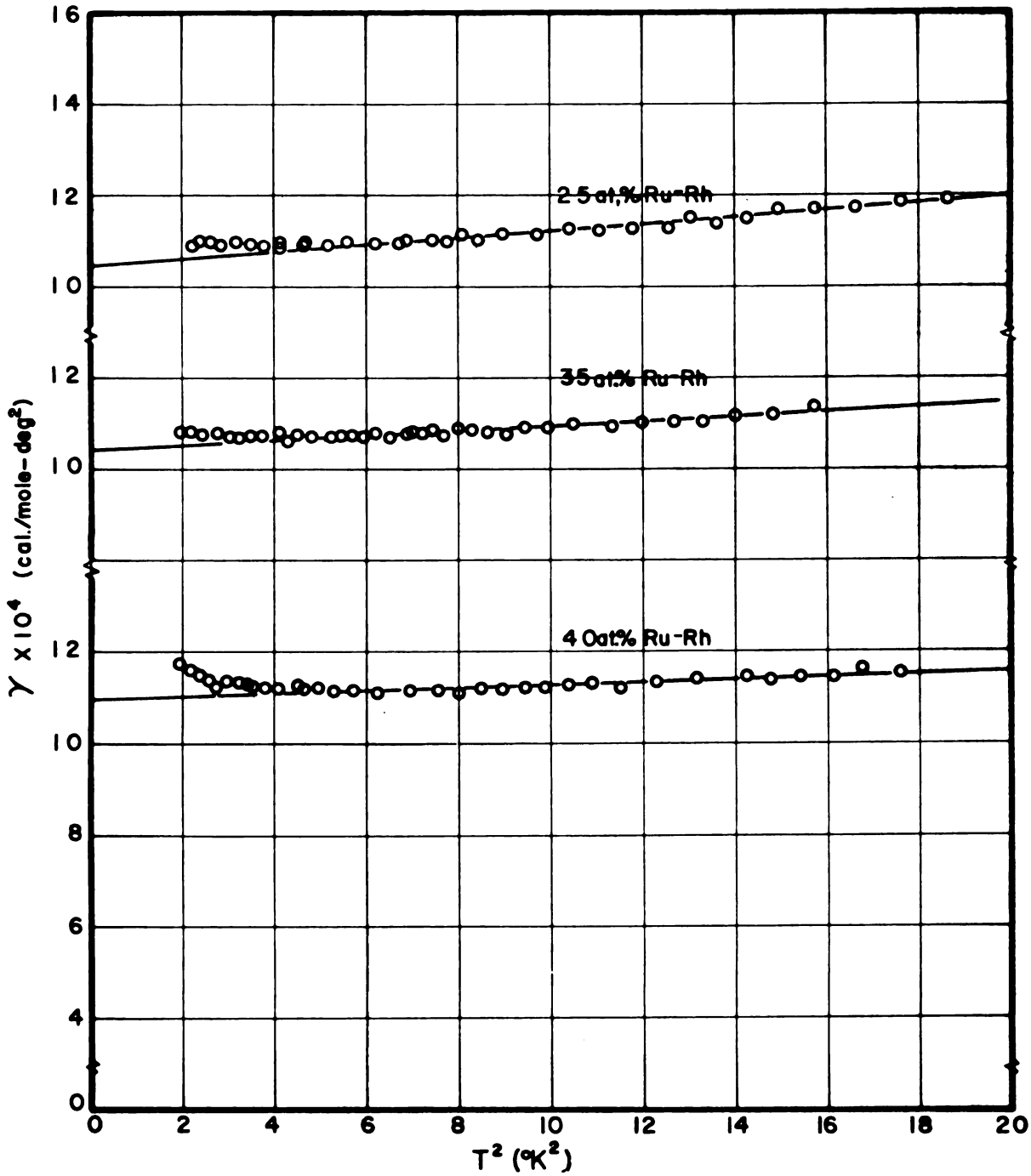

Fig. 3-4.--C_v/T vs T^2 Curves of Rh-Ru Alloys.

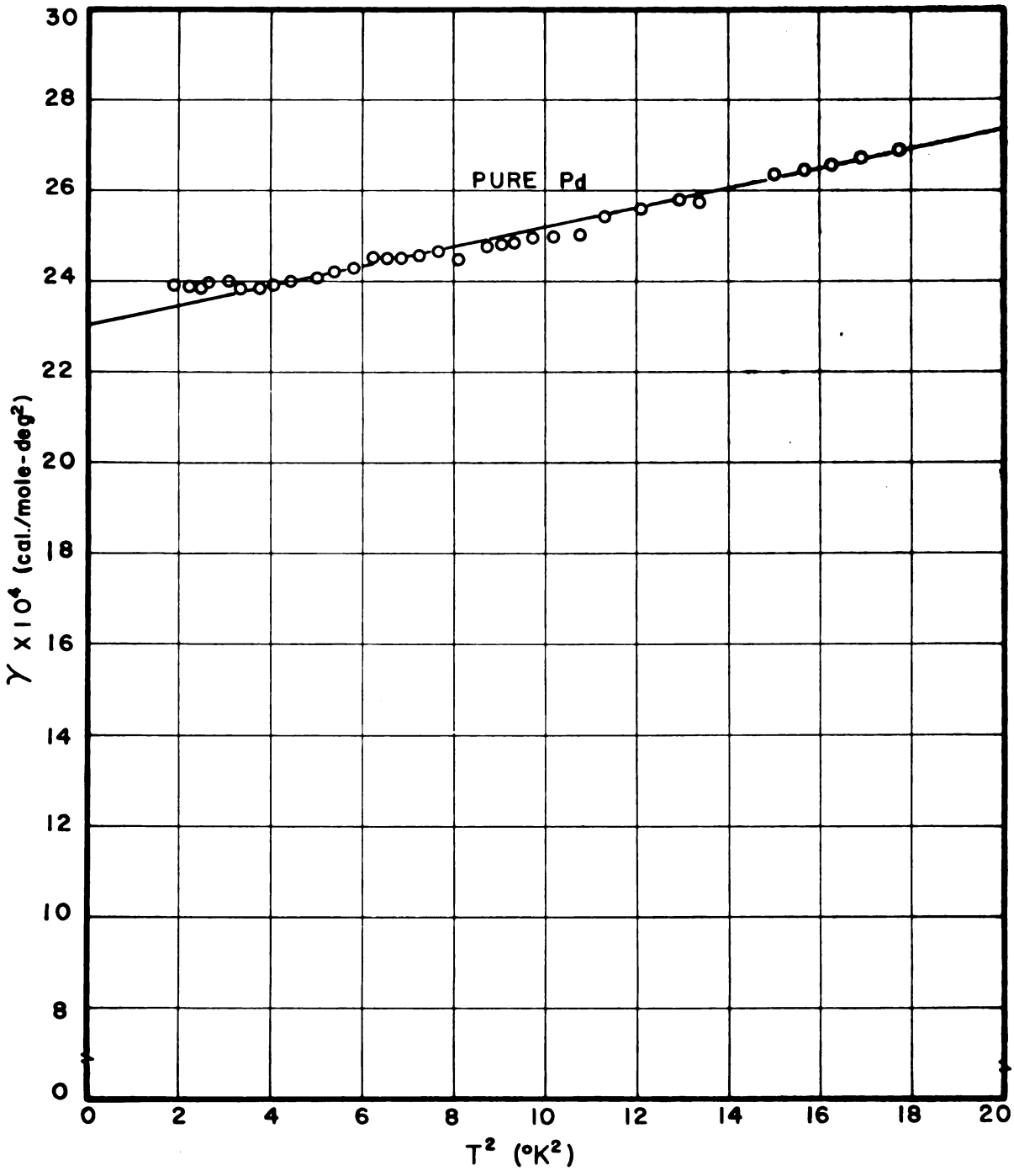

Fig. 3-5.--C_v/T vs T^2 Curve of Pure Pd.

The calculations were carried out with the Control Data 3600 computer using the program described in Appendix B-1.

The values of γ and θ thus obtained for all the alloys as well as pure Pd and Rh are listed in Table III-1.

Accuracy and Reproducibility of Results

The reliability of this investigation depended mainly upon the accuracy of the experimental results. In this section the experimental accuracy and the reproducibility of the results are to be examined.

Referring to equation (3-5), it can be seen that there are three sources of errors to be considered, namely, the accuracy in supplying the thermal energy i^2Rt, the accuracy in measuring the temperatures of the sample assembly, and the error introduced in assigning the heat capacity value and the molecular weight to the heater-thermometer assembly.

A. Inaccuracy in Thermal Energy Input, i^2Rt

Ai. Systematic error in the electrical system.--The limit of error for both standardizing and measuring in the lowest range of the K-3 potentiometer is ±0.015% of reading ±0.5 μV. The d-c null detector has a sensitivity of ±0.9 microvolts per division in the maximum sensitivity scale. Thus the inaccuracy introduced in the standardization of the K-3 potentiometer would be at most ±0.02%. The maximum inaccuracy in setting the heater and thermometer currents

TABLE III-1.--Values of γ and θ of Ru-Rh and Pd-Rh Alloys (Least Square Fit: $C_v/T = \gamma + \beta T^2$)

Alloy	$\gamma \times 10^4$ (cal./mole-deg^2)	θ (°K)
Pure Pd		
This work	23.01	278.28
Rayne*	25.6 ±1.3	--
Budworth et al.#	23.14	274.0 ±3.0
40 at. % Pd-Rh	14.94	397.46
30 at. % Pd-Rh	14.17	447.50
22 at. % Pd-Rh	13.99	498.41
15 at. % Pd-Rh	12.81	453.11
7 at. % Pd-Rh	12.01	451.89
Pure Rh		
This work	12.03	528.58
Budworth et al.#	11.56 ±0.07	512.0 ±17.0
5 at. % Ru-Rh	11.65	456.61
10 at. % Ru-Rh	11.30	429.77
15 at. % Ru-Rh	10.89	427.54
20 at. % Ru-Rh	10.97	454.74
25 at. % Ru-Rh	10.48	396.93
35 at. % Ru-Rh	10.40	444.27
40 at. % Ru-Rh	10.96	527.89

*J. Rayne, Phys. Rev. 95, 1428 (1954).

#D. W. Budworth, F. E. Hoare and J. Preston, Proc. Roy. Soc. (London) A257 (1960).

was perhaps ±0.01% in each case. The combined maximum possible error in the i^2Rt term due to the K-3 potentiometer and the d-c null detector would thus be ±0.05%.

The Beckman/Berkeley Model 5010 electronic counter has a capability of resolving one-volt pulses of 5μ sec. in width and with a separation of 25μ sec., and a counting rate of 0-12500 counts per second. The frequency standard has a frequency of 100 cps and an accuracy of 0.001%. The built-in inaccuracy of the counter is thus negligible. The accuracy of the measured heating time is ±0.0005 second. For the shortest heating period of 10 seconds, the corresponding maximum inaccuracy in the measured heating time was thus ±0.005%.

Since the time delay in the electronic switch was negligible, it was thus concluded that the total inaccuracy in the instrumentation was less than ±0.006%.

Aii. Errors introduced during the experiment.--The use of the electronic switch caused a deviation in the heating current of 0.8%, while the resistances of the four short pieces of manganin wires inserted between the copper leads and the measuring junctions on the kovar seal amounted to 1.3% of the total heater resistance. These two factors were taken into consideration in the calculation of the heat capacity of the sample assembly and hence would not introduce any error in the final results.

The resistance of the heater used in the calculation was the value measured at 4.2°K. However, from 4.2°K to 1.4°K the resistance of the heater decreased 0.05%. This

was the maximum error that could be caused by the variation in the heater resistance.

Therefore, the maximum total inaccuracy in the thermal energy input was less than ±0.11%.

B. Errors Due to the Inaccuracy in the Measurement of the Temperatures of the Sample Assembly

The accuracy of measuring the initial and final temperatures of the sample assembly before and after the heating period depended upon the accuracy of measuring the corresponding resistance R_1 and R_2 of the thermometer and the accuracy of the thermometer calibration. The following causes are to be considered.

Bi.--The accuracy of the d-c amplifier, which is ±0.4%, plus the accuracy of the K-3 potentiometer and the d-c null detector may result in a maximum systematic error of ±0.4005%.

Bii.--The smoothness and linearity of the branches of the heating curve corresponding to the thermal drift and the degree of exactness in extrapolating these branches to the mean-time line may cause an inaccuracy in the values of R_1 and R_2 by 0.15%.

Hence, Bi and Bii may cause a maximum error in R_1 and R_2 of about 0.43%.

Biii.--Inaccuracy of measuring the vapor pressure of the liquid helium bath.

a. The resolution of the cathetometer is ±0.01 mm. Taking the vapor pressure of liquid helium at 1.8°K for comparison, i.e., 10 mm Hg, this will introduce an inaccuracy in the measurement of ±0.1%. Due to human error, the inaccuracy can be as high as ±0.2%.

b. The maximum error in the hydrostatic pressure correction above the λ point is ±0.25%.

c. The error that may be introduced by the Stoke's gauge reading for pressure correction is negligible compared with the errors due to other sources.

The total inaccuracy in measuring the vapor pressure of the liquid helium is thus 0.32%. This may give rise to an error in the temperature of the liquid helium bath of 0.35%.

Therefore, the total uncertainty in the temperature measurement will be about ±0.7%. This will result in a maximum error of ±1.4% in ΔT, the temperature increment of the sample assembly after each heating, which may in turn introduce an error in the heat capacity of the sample assembly of approximately ±1.4%.

C. Errors Due to Other Sources

The errors due to the inaccuracies in calculating the molecular weight and the number of moles of each of the alloys were negligible. Since the combined weight of the

carbon thermometer and the other added materials in making the heater-thermometer assembly was only a small fraction of its total weight and the heat capacity of copper was much lower than those of the alloys, the heat absorbed by the heater-thermometer assembly as a whole is small. The error introduced in asigning the heat capacity and the molecular weight of the heater-thermometer assembly as being that of pure copper was thus also ignorable.

D. The uncertainty in the alloy composition was mainly caused by the metal loss during the melting operation. In the Ru-Rh alloys this uncertainty was less than 0.5% while in the Pd-Rh alloys it could have been as large as 1.0%.

As analyzed above, it may be concluded that the maximum experimental error that might be introduced in the final results was ±1.5%.

The reproducibility of the results were checked for two different cases: first, the reproducibility of the results after repeated heating and cooling in one experiment as can be seen in both of the curves in Fig. 3-6. Secondly, the reproducibility of the results obtained in different experiments with the same specimen; this is shown by plotting two sets of experimental data of the same sample in a single diagram, as also can be seen in Fig. 3-6. In addition, all

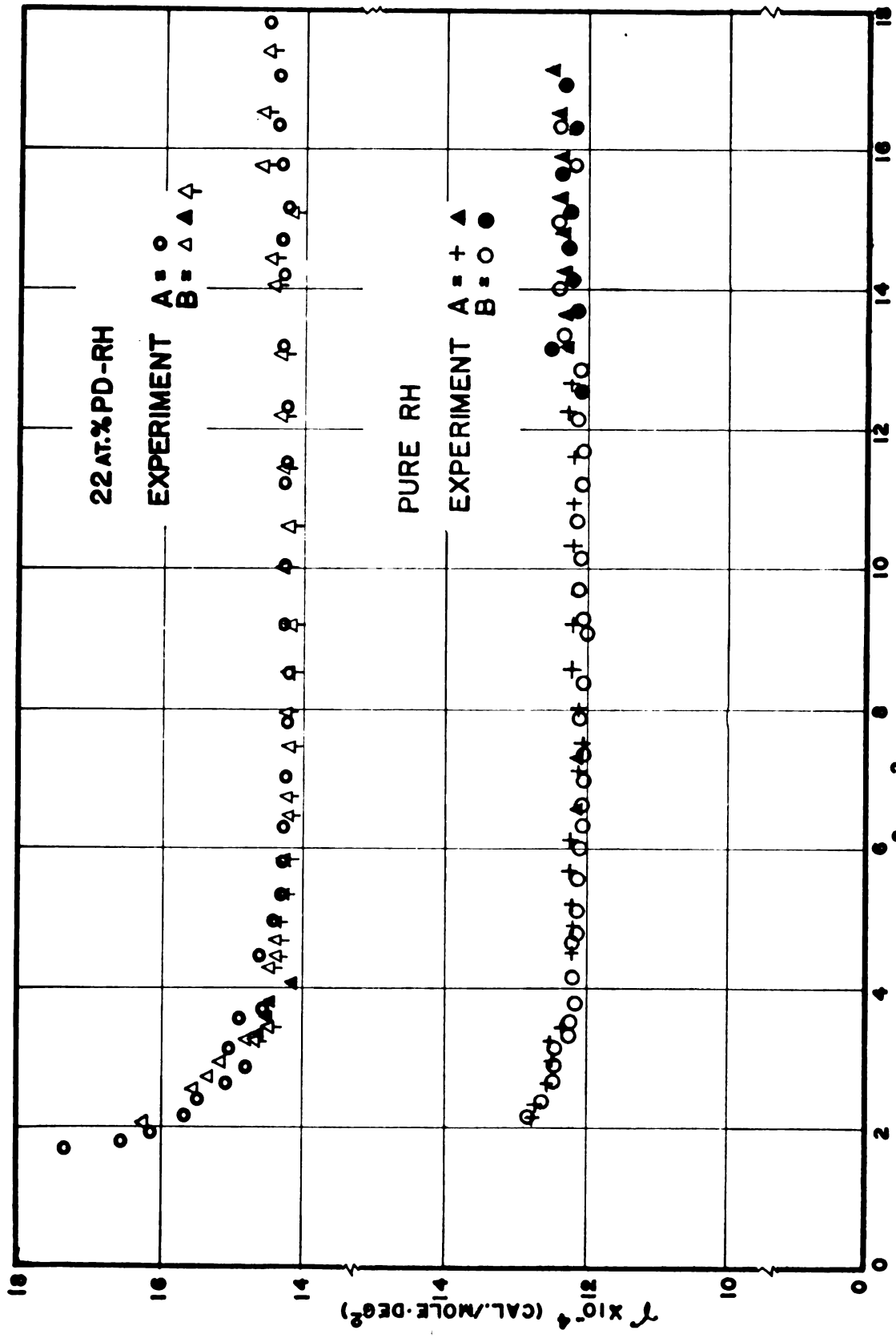

Fig. 3.6.--The experimental results of γ vs T^2 of 22at.% Pd-Rh and pure Rh in two experiments A and B. (Points fall well within the limit of experimental error.)

the points fall well within the limit of the experimental error in each case supporting the analyses of the probable error given above.

CHAPTER IV

DISCUSSION

A. Anomaly of the C_v/T versus T^2 Curves

As described in the previous chapter, the measured C_v's of each of the alloys were first calculated and fitted to the usual heat capacity equation, $C_v/T = \gamma T + \beta T^2$, by a least-squares method. Accordingly, a straight line with a slope related to the Debye temperature θ through Eq. (1-2) would be expected. For some of the Ru-Rh alloys straight lines were indeed obtained. However, conspicuous Schottky type anomalies were observed in those C_v/T versus T^2 curves of the other alloys, especially of those with compositions near 22 at .% Pd in Rh. It was intuitively suspected that experimental mistakes might have caused such a "curving-up" of the C_v/T versus T^2 curve at low temperatures. First of all it could be due to the evaporation of any condensed helium exchange gas on the surfaces of the sample assembly during the early period of the experiment. This possibility is considered unlikely in view of the following facts. (a) The vapor pressure of the helium exchange gas was originally 700 μ Hg at room temperature, it reduced to about 8 μ Hg at the lowest temperature of the liquid helium bath of 1.25°K. After being evacuated

continuously for one hour, the vacuum in the calorimeter at the beginning of the measurement was only 6.0×10^{-5} mm Hg. It is thus unlikely that there was still an appreciable amount of condensed helium gas left on the surface of the sample assembly. It is true that the vacuum in the calorimeter would eventually be improved and reach an end pressure of $6\text{-}8 \times 10^{-6}$ mm Hg as the experiment went on. This, however, was proved to be mainly due to the degassing of the conduit tube connecting the calorimeter can and the head housing of the calorimeter. (b) Some samples were first warmed up above the λ point of liquid helium, and left to be cooled gradually without introducing any additional exchange gas into the system so that most of the condensed helium, if any, would be evaporated from the surface of the sample assembly. The C_v's of the samples were then measured. It was found that the C_v/T versus T^2 curves obtained in this way were essentially the same as those obtained without prewarming. (c) No appreciable change of the vacuum in the system was observed during the heating period, as would be expected from a burst of gas in such a high vacuum condition.

The second possible experimental error that could cause such an anomaly would be the way to calculate the characteristic parameters of the thermometer. It was first thought that to fit the thermometer calibration curve to a polynomial including lnR terms of higher power would improve the linearity of the C_v/T versus T^2 curves. But just to

the contrary, the anomaly in the C_v/T versus T^2 curves was increased by such a non-linear fit of the calibration curve of the thermometer.

It seems clear from the above discussion that the "curving-up" of the C_v/T versus T^2 curves of some of the alloys at low temperatures was not a result of experimental error but due to some real contributions other than the electronic and lattice specific heats.

Anomaly of this type was first observed by Keesom et al. [64] in $Ni_{40}Cu_{60}$ alloy. Based on the fact that Ni is ferromagnetic they related this anomaly to an effect of magnetic in nature, although the alloy itself is paramagnetic. Similar anomalies were also observed by Wei et al. [65] in Ti-Fe and Fe-V alloys. In these alloys, the curving up of the C_v/T versus T^2 curves at low temperatures is obviously related to the content of the ferromagnetic element Fe. The greater the Fe content is the greater is the anomaly. Schröder and Cheng [66] suggested that there are ferromagnetic clusters existing in the alloys, and each cluster oscillates around an orientation determined by the energy of the crystal anisotropy. The cluster may thus contribute an additional term to the specific heat of the alloy. This "ferro-magnetic-cluster specific heat" is roughly independent of temperature in the experimental temperature range, and the low temperature specific heat of such an alloy may be expressed by [67]

$$C_v/T = \gamma + \beta T^2 + C'/T \qquad (4\text{-}1)$$

Where γ and β have the usual meaning while C' is the "ferro-magnetic-cluster specific heat" of the alloy. By assigning appropriate values to the Debye temperature of the alloys, Schröder fitted the data of Guthrie et al. [68] and that of Wei et al. [65] to $(C_v - C')/T = \gamma + \beta T^2$; obtaining straight $(C_v - C')/T$ versus T^2 curves.

Anomalies similar in appearance but of a different nature have been observed by Arp et al. [69, 70] in Co and Co-Fe alloys that are interpreted, however, by them and by Marshall [71] as a result of the hyperfine interaction between the magnetic moment of the nucleus and the effective magnetic field of the electrons at the nucleus.

In the Pd-Ag and Pd-Rh alloys, investigated by Hoare et al., no such anomalies were reported. But recently, such Schottky tail-type anomalies were observed in Pd-Ag alloys of compositions near 40 at.% Pd in Ag by Montgomery et al. [48]. Several possible causes were discussed by them. They seem to favor Schröder and Cheng's ferromagnetic cluster picture, but made no conclusion with certainty.

Reviewing the possible contributions to the low temperature specific heat other than those of the electronic and the lattice, it can be found that most of them fall in either of the following two groups: (a) those depend upon temperatures with a positive power, and (b) those depend upon temperatures with a negative power. Contributions

falling in group (a) are mostly due to magnetic effects, such as ferromagnetism ($C_{ferro.} \propto T^{2/3}$), antiferromagnetism ($C_{antiferro.} \propto T^{3}$), etc., while in group (b) nuclear specific heat is the most important one. Nuclear specific heat is attributed to the redistribution of the nuclear spins among the Zeeman energy levels [72], the "high-temperature tail" of which can be expressed as [71]

$$C_v/R = \frac{1}{3} I(I+1)(g_n\mu_n H/kT)^2 + O(g_n\mu_n H/kT)^4 + \ldots . \quad (4-2)$$

where I is the nuclear spin angular momentum, g_n is the Lande g factor for nucleus, μ_n is the nuclear magneton, and H is the total effective magnetic field.

The T^{-2} term is due to the hyperfine effect while the T^{-4} term is due to the dipole-dipole interaction. Generally only the T^{-2} term is taken into account. In most rare earth metals, it is found [73] that the nuclear specific heat predominates below 1°K.

None of the metals, Ru, Rh, and Pd, investigated in this experiment is ferromagnetic or antiferromagnetic when it is pure. Pd and Rh are non-superconducting, and the transition temperature of Ru is only 0.47°K, much too low for Ru to make an appreciable specific heat contribution in the temperature range of the present experiment. It is thus unlikely that the anomaly is due to the superconductivity of the alloy.

The curving-up effect itself suggests a contribution which is either independent of temperature, or dependent on temperature with a power less than unity. Among these known effects, the possible causes which may result in such "Schottky tail" type anomalies would either be the nuclear specific heat, depending on T^{-2}, or the specific heat due to ferromagnetic clusters as suggested by Schröder, a term that is independent of temperature in the experimental temperature range.

In order to check if any of the above effects were responsible for the low temperature anomaly, the experimental results were first fitted to an equation including a term of Schröder's magnetic specific heat:

$$C_v = A + \gamma T + \beta T^3 \qquad (4\text{-}3)$$

and then fitted to an equation with a nuclear specific-heat term (ignoring the T^{-4} term of the dipole-dipole interaction)

$$C_v = BT^{-2} + \gamma T + \beta T^3 \qquad (4\text{-}4)$$

The coefficients A, γ, and the corresponding Debye temperatures θ obtained from Eq. (4-3) are listed in Table IV-1, while the coefficients B, γ, and the Debye temperatures obtained by fitting to Eq. (4-4) are listed in Table IV-2. The values of γ and θ obtained by fitting the data to the

TABLE IV-1.--Coefficients of the least square fit to the equation: $C_v = A + \gamma T + \beta T^3$

Alloy at.% Ru-Rh	A x 10^4 (cal/mole-deg)	γ x 10^4 (cal/mole-deg^2)	θ(°K)
0.0	3.39	10.51	396.64
5.0	2.06	10.75	399.10
10.0	2.83	9.88	354.06
15.0	1.69	10.00	371.44
20.0	1.21	10.35	403.10
25.0	1.74	9.64	358.87
35.0	1.54	9.60	384.89
40.0	2.44	9.70	397.55
at. % Pd-Rh			
7.0	3.63	10.22	349.58
15.0	2.59	11.51	369.99
22.0	6.47	10.91	328.73
30.0	4.84	11.95	343.42
40.0	4.09	12.96	324.59

TABLE IV-2.--Coefficients for the equation: $C_v = BT^{-2} + \gamma T + \beta T^3$

Alloy at.% Ru-Rh	B x 10^4 (cal-deg/mole)	γ x 10^4 (cal/mole-deg^2)	θ($^\circ$K)
0.0	3.66	11.84	487.99
5.0	2.10	11.57	448.52
10.0	3.01	10.97	392.07
15.0	1.78	10.67	399.31
20.0	1.36	10.81	428.30
25.0	1.84	10.32	382.53
35.0	1.46	10.24	419.82
40.0	2.64	10.66	490.16
at. % Pd-Rh			
7.0	3.61	11.86	406.84
15.0	2.69	12.53	413.52
22.0	6.75	13.44	412.80
30.0	5.62	13.76	401.53
40.0	4.35	14.56	366.17

conventional equation (Eq. 1-1) and those by fitting to the above two equations (Eqs. 4-3 and 4-4), together with the results of Hoare et al. are all plotted against the electron concentrations, e/a, in Fig. 4-1. As can be seen the results obtained by fitting the data to the equations (1-1) and (4-4) do not differ appreciably from each other, show less scattering, and are more consistent with the results of Hoare et al. than those obtained by fitting to equation (4-3). A smooth continuous γ versus e/a curve is drawn in Fig. 4-1 that it may, perhaps, represent the upper part of 4d-band. It seems that the low temperature anomalies in the present results are not describable by Schröder's magnetic-cluster specific-heat. Although the results seem to suggest that the anomalous curving-up effect in the C_v/T versus T^2 curves of some of the Rh-Ru and Pd-Rh alloys would be attributable to the hyperfine interaction but, because of the experimental temperature range of this investigation is not low enough, it cannot be said with certainty that such is the case. Further investigation at temperatures below 1°K may help in clarifying this question.

B. Features of the γ Versus e/a Curve

As shown in Fig. 4-1, the γ versus e/a curve embraces both the results of Hoare et al. and those obtained in this investigation. Taking 10 to be the number of the outer electrons in palladium, the curve shows that after passing

a peak at e/a of 9.95 the γ decreases as the electron concentration, e/a, decreases until a e/a ratio of about 8.7 is reached, it then rises again as the e/a ratio decreases further.

C. Debye Temperatures of the Alloys

The Debye temperatures, θ, of the alloys are also plotted against the electronic concentrations, e/a, in Fig. 4-1. For the Pd-Rh alloys, θ decreases as the content of Pd increases, in agreement with the results of Hoare et al. A minimum is observed in the portion of the θ versus e/a curve of the Rh-Ru alloy system. The scattering of θ is rather large compared with that of the noble metal alloys. This is probably due to the irregular shape of 4-d band. According to Stoner [39], the electronic specific heat of a metal with energy band of irregular shape depends not only on the density of states at the Fermi level but also on the local slope and curvature of the energy band. An extra term depending on T^3 should be included in the electronic specific heat. This T^3 term is small compared with the term linear in T, and is usually ignored. Since the coefficient of the lattice specific heat is only 0.5% of that of the electronic specific heat, this T^3 term of the electronic specific heat which cannot be separated from the lattice specific heat might have affected the correct evaluation of the Debye temperatures of the alloys.

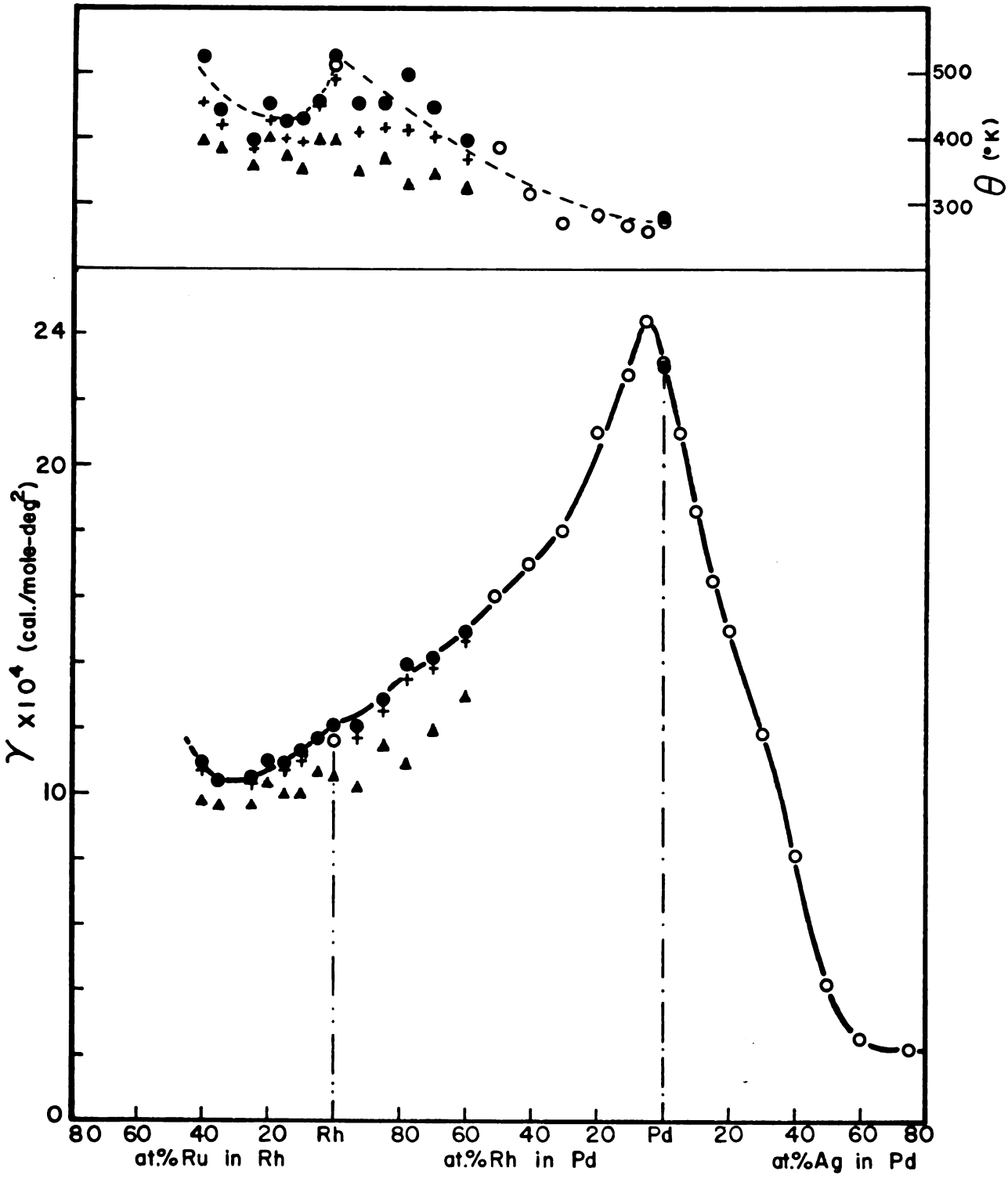

Fig. 4-1.--γ vs e/a curve. Soild dots represent results obtained by fitting to $C_v/T = \gamma + \beta T^2$, + are results fitted to $C_v = BT^{-2}+\gamma T+\beta T^3$, ▲ are results fitted to the equation: $C_v = A^v+\gamma T + \beta T^3$, while the open circles are results from Hoare et al.

D. N(E) Versus E Curve--the Upper Part of the 4d-Band

A density of states, N(E), versus energy, E, curve is more useful than the γ versus e/a curve.

The single spin density of states at the Fermi level of an alloy is calculated by using

$$N(E_f) = (3/\pi^2 k^2)\cdot\gamma. \qquad (4\text{-}5)$$

for γ expressed in units of 10^{-4} cal./mole-deg^2, Eq.(4-5) becomes

$$N(E_f) = 0.178\ \gamma. \qquad (4\text{-}5')$$

Where $N(E_f)$ is the single-spin density of states per eV at the Fermi level of the alloy. The number of electrons in a small energy interval ΔE near the Fermi level is approximately

$$\Delta n = \Delta E\ \overline{N(E_f)}. \qquad (4\text{-}6)$$

where $\overline{N(E_f)}$ is the average value of the density of states of two neighboring alloys, $N(E_{fa})$ and $N(E_{fb})$, i.e.,

$$\overline{N(E_f)} = \tfrac{1}{2}[N(E_{fa}) + N(E_{fb})]. \qquad (4\text{-}7)$$

Hence

$$\Delta E = \Delta n/\overline{N(E_f)}. \qquad (4\text{-}8)$$

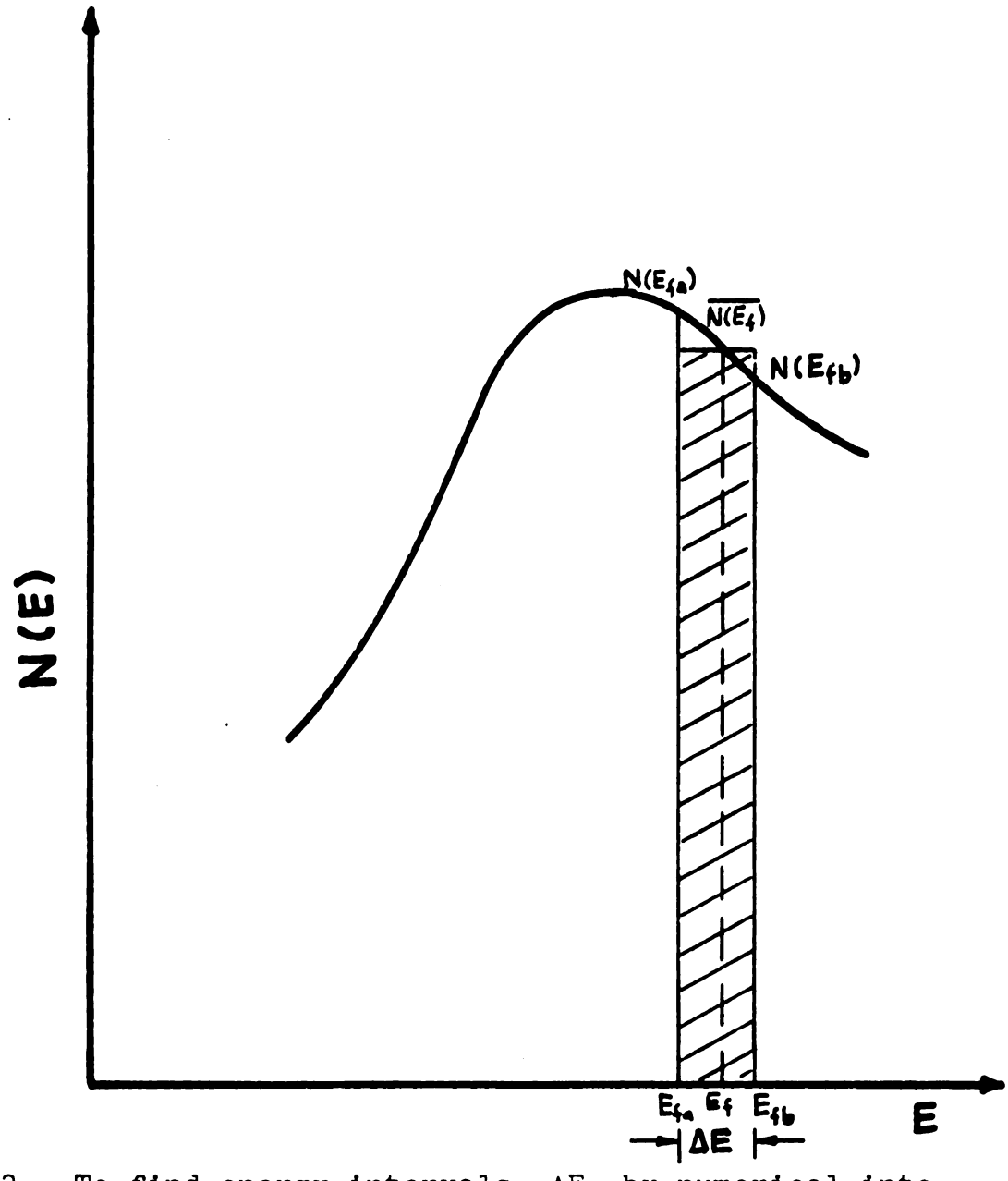

Fig. 4-2.--To find energy intervals, ΔE, by numerical integration. $N(E_{fa})$ and $N(E_{fb})$ are the density of states calculated from corresponding γ's of two neighboring alloys. $N(E_f) = \frac{1}{2}[N(E_{fa})+N(E_{fb})]$. The shaded area under the N(E) vs E curve equal to the number of electrons added to the alloy by increasing the solute content of an amount of Δc.

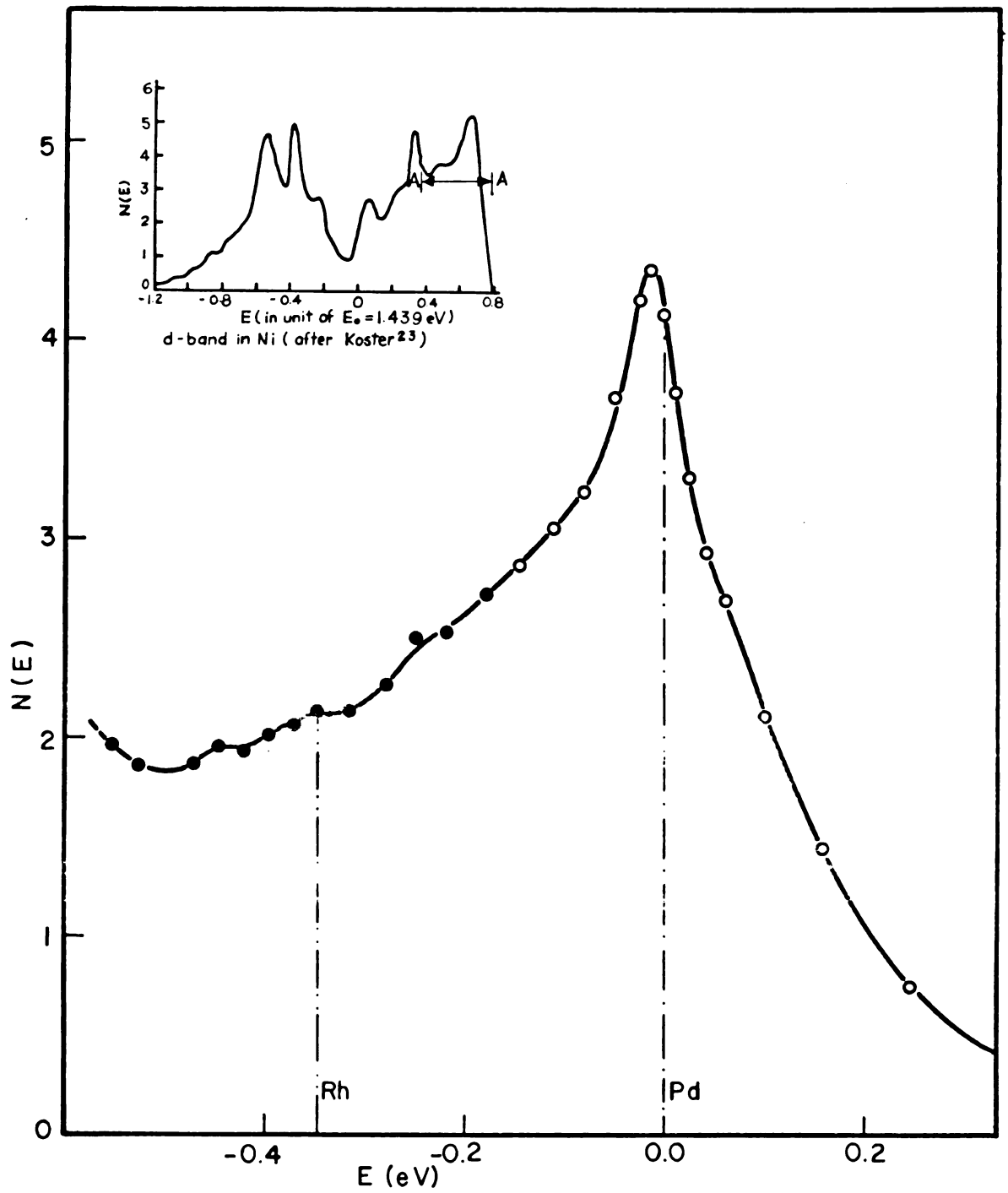

Fig. 4-3.--The upper part of the 4d-band deduced from the γ values of the fcc solid solution alloys of 2nd long period transition metals, i.e., Ru-Rh, Rh-Pd, and Pd-Ag alloys. Energy range covered corresponds to the A--A part of Koster's 3d-band.

Letting z be the number of electrons per atom added to the alloy per unit concentration change, and Δc be the increment of alloy concentration then,

$$\Delta E = z\Delta c/\overline{N(E_f)}. \qquad (4\text{-}9)$$

Strictly speaking, z is a function of c and should be determined by other experiments. But to a first approximation, z can be taken as the relative valency of the two constituent metals of the alloy. Thus z = 1.0 for adding Pd to Rh or by alloying Rh to Ru. Figure 4-2 shows schematically the numerical method to find the energy intervals, ΔE.

Together with the data of Hoare et al., a density of states versus energy curve is thus constructed, and is shown in Fig. 4-3. It should be pointed out that the energy band shown in Fig. 4-3 is the total density of states of the d-electrons as well as the s-electrons, since the heat capacity measured experimentally includes the contributions from both of them. However, the density of states of the 5s electrons is much less than that of 4d's; its contribution to the heat capacity is, consequently, very small. Furthermore, the energy range covered in this investigation is small ($\sim$0.8 eV) compared with the entire width of the 5s band ($\sim$ 13 eV). The density of states of 5s band may thus be regarded as being more or less constant over the entire experimental energy range. Therefore, the

general features of the N(E) versus E curve shown in Fig. 4-3 can be considered as representing the general features of the upper part of the 4d-band in the fcc structure. As can be seen, to the left of the high peak, the density of states decreases as the Fermi surface moves toward lower and lower energy as observed by Hoare [53], and then bends upward again at about 0.5 ev below the Fermi level of pure palladium. This last feature may be of significance in correlating the experimental results to the theoretical 4d-bands.

The "d-hump" in the total energy band of fcc copper calculated by Burdick [14] using the APW method bears a peak with no "valley" in the middle, whereas a conspicuous "valley" is shown in the fcc d-band calculated by using the tight-binding method. Mott [32] seems to prefer the former picture, while others regard the tight-binding method should be the more appropriate one for treating the d-electrons. To decide which method is more appropriate should be important for the formulation of the electronic structure of transition metals, especially in those aspects related to the occurrence of ferromagnetism. The "bending-up" feature provides a clue to the belief that there is a "valley" in the middle of the d-band for the fcc structure, and hence the tight-binding method might be the more appropriate one.

To compare the 4d-band obtained in the present investigation with those obtained from tight-binding calculations,

the 3d-band of fcc Ni calculated by Koster [25] is plotted at the upper left of Fig. 4-3. As can be seen, present experimental 4d-band bears a fair resemblance with the upper part of Koster's curve. Resemblance can also be found between the experimental 4d-band and the 4d-band of palladium calculated by Lenglart et al. [31], using also the tight-binding method, although for accommodating the same number of electrons the energy range covered in the band of Lenglart et al. is much smaller while the density of states in the same energy range is much larger than that in the experimental band. The introducing of the spin-orbital interaction by Lenglart et al. might have caused these deviations. Due to the discovery of s-electrons in pure palladium [51], it is thought that the hybridization of s-d electrons would alter the total band structure drastically. This is shown to be perhaps not so in view of Mueller's band calculation [34]. By using an interpolation scheme, Mueller found that although s-d hybridization does change the d-band to some extent yet the main features of a tight-binding d-band are still retained. The experimental d-band of this investigation appears to match even better with Mueller's results than with Koster's in the height of the band and the energy range covered. Since the comparison is at best qualitative, it would not be possible to draw a positive conclusion about whether or not Mueller's interpolation scheme is closer to the truth. Nonetheless,

the tight-binding scheme is still employed in constructing the total d-wave functions in Mueller's method and one may conclude that for the d-bands in the transition metals, the tight-binding approximation is essentially correct, at least for constructing the total d-wave functions. The 4d-band of palladium and that of silver obtained by Yu and Spicer [74] and Spicer [75] respectively using an optical method also show the features of a tight-binding d-band. The present results support this recognition.

E. Applicability of the Rigid-Band Model to Alloys of the Transition Metals

In calculating the N(E) versus E curve from the specific heat data a rigid-band is implied. There has been no proof of the general applicability of such a model. Perhaps the first question to be asked is: would adding an alloying element change the band structure drastically? Considering from the first principles applied to the energy band calculations, and confining the case to binary alloys of neighboring transition elements in the same long period in the periodic table, the answer would be negative, since the lattice potentials (self-consistent field of the element) of the neighboring elements in the same period are more or less the same, and the periodicity of the lattice potential would still be retained in the alloys. The wave functions in the alloy would still be of Bloch type and be more or less the same as that in pure

metals. Therefore, alloying such as described will introduce only a small perturbation which may not alter the essential features of the resulting band. Mattheiss' calculation [12] provides a theoretical justification for this point.

It is known that the relative position of the s and d bands of two neighboring transition metals may vary. Thus it is natural to ask a second question : whether or not the change of the relative position of the s-d bands would cause a large change in the major features of the total density of states curve of the alloy? The answer is, according to Mueller [45], also negative.

The theories are therefore in favor of the applicability of the rigid-band model. Experimentally, the agreement between 4d-band derived from the specific-heat data and that calculated theoretically seems to suggest that the rigid-band model may indeed have some truth in applying to the restricted alloys of the transition metals.

CHAPTER V

CONCLUSIONS

(1). The solubility limit of Ru in fcc Rh was found, by using an X-ray diffraction method, to be between 40 and 42 at.% Ru.

(2). The specific heats of 14 samples, including 12 fcc Ru-Rh and Rh-Pd solid-solution alloys and one of each of pure rhodium and pure palladium, were measured between 1.4 and 4.2°K. The coefficients of γ of the electronic specific heats of pure Rh and pure Pd determined by the present work agree with those obtained by previous investigators within the limit of the experimental error.

(3). A "Schottky-tail" type anomaly was observed in some of the alloys especially in those with composition near 22 at.% Pd in Rh. The cause of this anomaly has not been established unambiguously. However, by fitting the experimental data to various equations representing the different solid state phenomena which might cause such an anamoly, it seems that the hyperfine interaction is the probable cause.

(4). A plot of the coefficient of the electronic specific heat γ versus the outer electron concentration e/a for the samples investigated in the present work joins smoothly with the existing results of Hoare et al.

(5). The uncertainty in the Debye temperatures of these alloys was found to be large compared with that of the alloys of the noble metals. A possible explanation is that this uncertainty is due to the effect of the local slope and curvature of the total density-of-states curves of the highly irregular 4d-band.

(6). A density-of-states curve constructed numerically for the upper part of the 4d-band from the experimental γ values is found to be in qualitative agreement with the corresponding part of the theoretical 3d-band calculated for the paramagnetic Ni by G. F. Koster using the tight-binding method. It appears that for the fcc structures the 4d-band of the second long period transition metals is similar to the 3d-band of the first long period transition metals, and that the approximate method of Linear Combination of Atomic Orbitals is essentially correct for treating the d-electrons in the transition metals.

REFERENCES

1. C. Kittel, "Introduction to Solid State Physics," Wiley and Sons (1967).

2. J. C. Slater, Phys. Rev., 49, 537 (1936).

3. L. Pauling, Phys. Rev. 54, 899 (1938); Proc. Natl. Acad. Sci. 39, 551 (1953).

4. J. H. Vleck, Rev. Modern Phys., 25, 220 (1953).

5. N. F. Mott and K. W. H. Stevens, Phil. Mag., 2, 1364 (1957).

6. W. M. Lomer and W. Marshall, Phil. Mag. 3, 185 (1958).

7. C. Herring, J. Appl. Phys., 31, 3S (1960).

8. T. L. Louks, "Augmented Plane Wave Method," Benjamin, New York (1967).

9. H. Jones, "The Theory of Brilloin Zones and Electronic States in Crystals," North-Holland (1962) Chap. 6.

10. H. M. Krutter, Phys. Rev., 48, 664 (1935).

11. J. C. Slater, Phys. Rev., 51, 846 (1937).

12. J. C. Slater, Phys. Rev., 92, 603 (1953).

13. M. M. Saffren and J. C. Slater, Phys. Rev., 92, 1126 (1953).

14. G. A. Burdick, Phys. Rev., 129, 138 (1963).

15. M. F. Manning, Phys. Rev., 63, 190 (1943).

16. J. B. Greene, Phys. Rev., 63, 203 (1943).

17. J. G. Hanus, Solid State and Molecular Theory Group, MIT, Quarterly Progress Report No. 44, p. 29 (1962).

18. T. L. Louks, Phys. Rev., 139, A1181 (1965).

19. L. F. Mattheiss, Phys. Rev., 134, 192 (1964).

20. J. H. Wood, Phys. Rev., 126, 157 (1962).

21. C. H. Cheng, C. T. Wei and P. A. Beck, Phys. Rev., 120, 426 (1960).

22. L. F. Mattheiss, Phys. Rev., 139, A1893 (1965).

23. G. C. Fletcher, Proc. Phys. Soc. Lond., A65, 192 (1952).

24. J. C. Slater and G. F. Koster, Phys. Rev., 94, 1498 (1954).

25. G. F. Koster, Phys. Rev., 98, 901 (1955).

26. E. I. Belding, Phil. Mag., 4, 1145 (1959).

27. M. Asdente and J. Friedel, Phys. Rev., 124, 384 (1961).

28. E. Abate and M. Asdente, Phys. Rev., 140, A1303 (1965).

29. J. Yamashita, M. Mukuchi and S. Wakoh, J. Physical Soc., Japan, 18, 999 (1963).

30. J. Friedel, P. Lenglart and G. Leman, J. Phys. Chem. Solids, 25, 781 (1964).

31. P. Lenglart, G. Leman and J. P. Lelieur, J. Phys. Chem. Solids, 27, 377 (1966).

32. N. F. Mott, Advances in Physics, 13, No. 51, 325 (1964).

33. L. Hodges, H. Ehrenreich and N. D. Lang, Phys. Rev., 152, 505 (1966).

34. F. M. Mueller, Phys. Rev., 153, 659 (1967).

35. J. B. Ketterson and Y. Eckstein, Phys. Rev., 140, A1355 (1965).

36. A. J. Blodgett, Jr. and W. E. Specier, Phys. Rev., 146, 390 (1966); C. N. Berglund and W. E. Specier, Phys. Rev., 136, A1030 (1966).

37. M. Born and J. R. Openheimer, Ann. Physik 84, 457 (1927); also see F. Seitz, "The Modern Theory of Solids," McGraw Hill (1940), chpt. 14.

38. Sommerfeld, Z., Ann. d. Physiks, 28, 1 (1937).

39. E. C. Stoner, Proc. Roy. Soc. (London), A154, 656 (1936).

40. M. H. Cohen and V. Heine, Advances in Physics, 7, 395 (1958).

41. S. Raimes, J. Phys. Radium, 23, 639 (1962).

42. J. A. Rayne, Phys. Rev., 108, 22 (1957); 110, 606 (1958).

43. J. C. Beeby, Phys. Rev., 135, A 130 (1964).

44. L. F. Matheiss, Phys. Rev., 134, A970 (1964).

45. K. P. Gupta, C. H. Cheng and P. A. Beck, J. Phys. Radium, 23, 721 (1962).

46. D. W. Budworth, F. E. Hoare and J. Preston, Proc. Roy. Soc. (London), A257, 250 (1960).

47. F. E. Hoare and B. Yates, Proc. Roy. Soc., (London), A240, 42 (1957).

48. H. Montgomery, G. P. Pells and E. M. Wray, to be published in Proc. Roy. Soc. (London).

49. H. Montgomery, unpublished, also see in Hoare's paper (48).

50. C. A. Mackliet and A. I. Schindler, Phys. Rev., 146, 463 (1966).

51. J. J. Vuillemin and M. G. Priestley, Phys. Rev. Letters, 14, 307 (1965).

52. H. Kimura, A. Katsuki and M, Shimizu, J. Physical Soc., Japan, 21, 307 (1966).

53. F. E. Hoare, "Electronic Structures and Alloy Chemistry of the Transition Elements," P. A. Beck ed., Interscience (1963), chap. 2.

54. For various methods see: J. M. Ziman, "Principles of the Theory of Solids," Cambridge Univ. Press (1964).

55. (a) R. I. Jaffee, D. J. Makuth and R. W. Douglass, "Ruthenium and the Refractory Platium Group Metals," A.I.M.E. Metallurgical Conferences, 1961, II, 383; (b) A. Hellawell and W. Hume-Rothery, Phil. Mag. 45, 797 (1954).

56. INCO Bulletin: Rhodium, p. 7 (1963), The International Nickel Co., Inc.

57. E. Raub, "Metals and Alloys of the Platium Group," J. Less Common Metals, I, 3 (1959).

58. E. Raub, H. Beeskow and D. Manzel, Z. Metallkude, 50, 428 (1959).

59. C. T. Wei, Ph.D. Thesis, Univ. of Illinois (1958).

60. P. H. Keesom and N. Pearlman, Encyclopdia of Physics, S. Fluge, ed., 14, 297 (1956); Corak, Garfunkel, Satterwaite and Wexler, Phys. Rev., 98, I699 (1955).

61. NBS Monograph 10, "The 1958 He^4 Scale of Temperatures," H. van Dijk, M, Durieux, J. R. Clement and J. K. Logan, ed. (1960).

62. Friedberg, Estermann and Goldman, Phys. Rev., 85, 735 (1952); Ibid. 87, 582 (1952), also see J. G. Daunt, "Progress in Low Temperature Physics," C. J. Gorter, ed., North-Holland, Amsterdam (1955), chap. XI, p. 208.

63. N. F. Mott and H. Jones, "The Theory of the Properties of Metals and Alloys," Table III, Dover (1958).

64. W. H. Keeson and B. Kurrelmeyer, Physica, 7, 1003 (1940).

65. C. T. Wei, C. H. Cheng and P. A. Beck, Phys. Rev., 120, 426 (1960).

66. K. Schröder and C. H. Cheng, J. Appl. Phys., 31, 2154 (1960).

67. K. Schröder, Phys. Rev., 32, 880 (1961).

68. G. L. Guthrie, S. A. Friedberg and J. E. Goldman, Phys. Rev., 113, 45 (1959).

69. V. Arp, N. Kurti and R. Pertsen, Bull. Am. Phys. Soc., 2, 388 (1959).

70. V. Arp, D. Edmonds and R. Perterson, Phys. Rev. Letters, 3, 212 (1959).

71. W. Marshall, Phys. Rev., 110, 1280 (1958).

72. A. J. Freeman and R. E. Watson, "Hyperfine Interaction in Magnetic Materials," in Magnetism IIA, ed. by Rado and Suhl.

73. O. V. Lounasmaa and L. J. Sundstrom, Phys. Rev., 150, 399 (1966); and the references in this article.

74. A. V. C. Yu and W. E. Spicer, Phys. Rev. Letters, 17, 1171 (1966).

75. W. E. Spicer, J. Appl. Phys., 37, 947 (1966).

APPENDICES

APPENDIX A

EXPERIMENTAL DATA

APPENDIX A:EXPERIMENTAL DATA

A-1 Pure Rhodium First Run

Weight of Alloy: 28.9723 gm No. of Moles: 0.2815

Weight of Heater-Thermometer Assembly: 3.4871 No. of Moles: 0.0349

Resistance of Heater at 4.2°K: 270.94 ohm

Thermometer calibration parameters: A = -1.016970
B = 0.626236

No. of Point	T (°K)	T^2 (°K^2)	C_v (cal./mole-deg)	C_v/T (cal/mole/deg^2)
1	1.4814	2.1946	0.0018997	0.0012824
2	1.5441	2.3844	0.0019840	0.0012848
3	1.6306	2.6590	0.0020712	0.0012702
4	1.7193	2.9561	0.0021709	0.0012626
5	1.8047	3.2568	0.0022834	0.0012653
6	1.8811	3.5385	0.0023480	0.0012482
7	1.9532	3.8151	0.0025150	0.0012876
8	2.0295	4.1187	0.0025870	0.0012747
9	2.1308	4.5401	0.0026305	0.0012345
10	2.2213	4.9341	0.0027426	0.0012347
11	2.2933	5.2593	0.0028342	0.0012359
12	2.3919	5.7210	0.0029653	0.0012398
13	2.4739	6.1200	0.0030641	0.0012386
14	2.6758	7.1598	0.0032790	0.0012254
15	2.7529	7.5787	0.0033705	0.0012243
16	2.8376	8.0521	0.0034887	0.0012294
17	2.9322	8.5980	0.0036035	0.0012289
18	3.0418	9.2528	0.0037492	0.0012325
19	3.1289	9.7902	0.0038570	0.0012327
20	3.2233	10.3893	0.0039667	0.0012306
21	3.3123	10.9710	0.0040923	0.0012355
22	3.4071	11.6084	0.0042153	0.0012372
23	3.4994	12.2461	0.0043483	0.0012426
24	3.5563	12.6475	0.0044099	0.0012400
25	2.5710	6.6103	0.0031590	0.0012287
26	2.7112	7.3507	0.0033342	0.0012298
27	3.7631	14.1609	0.0047011	0.0012493
28	3.6308	13.1829	0.0045064	0.0012412
29	3.6999	13.6892	0.0046109	0.0012462
30	3.7719	14.2273	0.0046751	0.0012394
31	3.8516	14.8351	0.0048129	0.0012496
32	3.9166	15.3399	0.0049148	0.0012549
33	3.9887	15.9096	0.0049858	0.0012500
34	4.0675	16.5445	0.0051081	0.0012558
35	4.1425	17.1606	0.0052443	0.0012660

Least Square Fit of Points from No.20 to No.35

γ = 0.0012028990 cal./mole-deg^2
β = 0.0000031434 cal./mole-deg^2
Θ = 528.583 °K

$C_v = 12.029T + 0.0314T^3$ (cal./mole-deg) $X10^{-4}$

A-2 5 At.% Ru-Rh

Weight of Alloy: 23.8421 gm No. of Moles: 0.2319

Weight of Heater-Thermometer Assembly: 5.2626 No. of Moles: 0.0828

Resistance of Heater at 4.2 K: 255.195 ohm

Thermometer calibration parameters: A = -1.025886
B = 0.637435

No. of Point	T (°K)	T^2 ($°K^2$)	C_v (cal/mole-deg)	C_v/T (cal/mole/deg^2)
1	1.4032	1.9691	0.0017186	0.0012248
2	1.4291	2.0424	0.0017346	0.0012138
3	1.4585	2.1274	0.0018313	0.0012556
4	1.4964	2.2392	0.0018607	0.0012435
5	1.5348	2.3556	0.0019086	0.0012436
6	1.5844	2.5104	0.0019493	0.0012303
7	1.6266	2.6459	0.0019722	0.0012125
8	1.6637	2.7679	0.0019801	0.0011902
9	1.6968	2.8792	0.0020657	0.0012174
10	1.7409	3.0306	0.0021141	0.0012144
12	1.8548	3.4403	0.0022342	0.0012045
13	1.9314	3.7304	0.0023308	0.0012068
14	2.0147	4.0590	0.0024352	0.0012087
15	2.1361	4.5628	0.0025863	0.0012108
16	2.1911	4.8007	0.0026429	0.0012062
17	2.2751	5.1762	0.0027487	0.0012081
18	2.3832	5.6796	0.0028830	0.0012097
19	2.5037	6.2685	0.0030215	0.0012068
20	2.5415	6.4591	0.0030561	0.0012025
21	2.6123	6.8243	0.0031435	0.0012033
22	2.6952	7.2640	0.0032325	0.0011994
23	2.7886	7.7764	0.0033714	0.0012090
24	2.8988	8.4033	0.0034930	0.0012050
25	2.9934	8.9603	0.0035991	0.0012023
26	3.0643	9.3902	0.0037061	0.0012094
27	3.1454	9.8938	0.0038110	0.0012116
28	3.2347	10.4633	0.0039365	0.0012170
29	3.3288	11.0810	0.0040189	0.0012073
30	3.3985	11.5495	0.0041753	0.0012286
31	3.4942	12.2092	0.0042722	0.0012226
32	3.6067	13.0080	0.0044146	0.0012240
33	3.6990	13.6826	0.0045775	0.0012375
34	3.7829	14.3101	0.0046631	0.0012327
35	3.8764	15.0263	0.0048041	0.0012393
36	3.9794	15.8356	0.0049582	0.0012460
37	4.0916	16.7415	0.0051087	0.0012486

Least Square fit of points from point No.21 toNo.37

γ =0.0011648541 cal./mole-deg^2
β =0.0000048769 cal./mole-deg^2
θ =456.605°K

$C_v = 11.649T + 0.0488T^3$ (cal./mole-deg) X 10^{-4}

A-3 10 at.%Ru-Rh

Weight of Alloy: 29.4333 gm No. of Mole: 0.2865

Weight of Heater-Thermometer Assembly: 5.2136 No. of Moles: 0.082

Resistance of Heater at 4.2 K: 256.145 ohm

Thermometer calibration parameters: A=-1.016366
B=0.6338952

No. of Point	T (K)	T^2 (K^2)	C_v (cal/mole-deg)	C_v/T (cal/mole-deg^2)
2	1.4217	2.0213	0.0017358	0.0012209
3	1.4379	2.0676	0.0017476	0.0012154
4	1.4852	2.2058	0.0017898	0.0012051
5	1.5444	2.3850	0.0018322	0.0011846
6	1.5883	2.5226	0.0019003	0.0011965
7	1.6511	2.7261	0.0019381	0.0011738
8	1.7270	2.9826	0.0020313	0.0011762
9	1.8023	3.2482	0.0021261	0.0011797
10	1.9390	3.7596	0.0022617	0.0011664
11	2.0358	4.1444	0.0023832	0.0011706
12	2.1500	4.6225	0.0025199	0.0011721
13	2.2470	5.0490	0.0026131	0.0011629
14	2.3245	5.4031	0.0027160	0.0011685
15	2.4443	5.9745	0.0028682	0.0011734
16	2.4900	6.2000	0.0028977	0.0011638
17	2.5549	6.5273	0.0029805	0.0011666
18	2.6253	6.8923	0.0030500	0.0011618
19	2.7055	7.3197	0.0031663	0.0011703
20	2.7955	7.8148	0.0032810	0.0011737
21	2.8949	8.3805	0.0033956	0.0011729
22	2.9994	8.9962	0.0035015	0.0011674
23	3.0682	9.4139	0.0036208	0.0011801
24	3.1469	9.9029	0.0037271	0.0011844
25	3.2286	10.4255	0.0038218	0.0011836
26	3.3263	11.0642	0.0040291	0.0012113
27	3.4388	11.8254	0.0040220	0.0011697
28	3.5493	12.5977	0.0042516	0.0011979
29	3.6387	13.2399	0.0043790	0.0012035
30	3.7214	13.8491	0.0045238	0.0012156
31	3.8341	14.7000	0.0046609	0.0012157
32	3.9284	15.4325	0.0048163	0.0012260
33	4.0588	16.4739	0.0050003	0.0012320
34	4.1517	17.2363	0.0051342	0.0012366
35	4.2403	17.9805	0.0052470	0.0012370

Least Square Fit of points from No.12 to No.35.

γ = 0.0011291913 cal./mole-deg^2
β = 0.0000058489 cal./mole-deg^2
θ = 429.766°K

$C_v = 11.292T + 0.0585T^3$ (cal./mole-deg) X 10^{-4}

A-4 15 at.% Ru-Rh

Weight of Alloy: 28.2757 gm No. of Mole: 0.2755

Weight of Heater-Thermometer Assembly: 5.2491 No. of Mole: 0.0826

Resistance of Heater at 4.2°K : 256.105 ohm

Thermometer calibration parameters: A = -1.015527
B = 0.633414

No. of Point	T (°K)	T^2 ($°K^2$)	C_v (cal/mole-deg)	C_v/T (cal/mole-deg^2)
1	1.4876	2.2129	0.0016659	0.0011198
2	1.5252	2.3263	0.0017223	0.0011292
3	1.5666	2.4544	0.0017666	0.0011276
4	1.6207	2.6267	0.0018312	0.0011299
5	1.6486	2.7180	0.0018581	0.0011271
6	1.6748	2.8048	0.0018872	0.0011268
7	1.7366	3.0158	0.0019530	0.0011246
8	1.7788	3.1641	0.0019917	0.0011197
9	1.8182	3.3059	0.0020491	0.0011270
10	1.8636	3.4730	0.0020950	0.0011242
11	1.9414	3.7691	0.0021871	0.0011265
12	2.0385	4.1556	0.0023043	0.0011304
13	2.0958	4.3926	0.0023676	0.0011297
14	1.9007	3.6127	0.0021158	0.0011132
15	2.1278	4.5275	0.0023830	0.0011199
16	2.2033	4.8547	0.0024731	0.0011224
17	2.2798	5.1974	0.0025592	0.0011226
18	2.4035	5.7767	0.0027028	0.0011245
19	2.4416	5.9614	0.0027571	0.0011292
20	2.4996	6.2488	0.0028028	0.0011212
21	2.5614	6.5609	0.0028873	0.0011272
22	2.6258	6.8946	0.0029654	0.0011294
23	2.7416	7.5163	0.0030850	0.0011253
24	2.8953	8.3827	0.0033016	0.0011403
25	3.0051	9.0305	0.0034061	0.0011335
26	3.0671	9.4069	0.0034904	0.0011380
27	3.1444	9.8873	0.0036336	0.0011556
28	3.2438	10.5221	0.0037614	0.0011596
29	3.3448	11.1875	0.0038192	0.0011419
30	3.4452	11.8698	0.0039323	0.0011414
31	3.5606	12.6778	0.0041068	0.0011534
32	3.6372	13.2295	0.0042165	0.0011593
33	3.7150	13.8013	0.0042975	0.0011568
34	3.7858	14.3320	0.0044749	0.0011820
35	3.8537	14.8513	0.0046036	0.0011946
36	3.9316	15.4578	0.0046590	0.0011850
37	4.0179	16.1439	0.0048324	0.0012027
38	4.1019	16.8255	0.0048990	0.0011943
39	4.2072	17.7007	0.0050222	0.0011937

Least Square Fit of Points from No. 13 to No. 35

γ = 0.0010893089 cal./mole-deg^2
β = 0.0000059407 cal./mole-deg^2
θ = 427.543°K

$C_v = 10.893T + 0.0594T^3$ (cal./mole-deg) X 10^{-4}

A-5 20 at.% Ru-Rh

Weight of Alloy: 29.2794 gm No. of Mole: 0.2855

Weight of Heater-Thermometer Assembly: 5.3897 No. of Mole: 0.0848

Resistance of Heater at 4.2°K : 255.16 ohm

Thermometer calibration parameters: A = -1.027808
B = 0.637368

No. of Point	T (K)	T^2 (K^2)	C_v (cal/mole-deg)	C_v/T (cal/mole-deg^2)
1	1.4325	2.0521	0.0016658	0.0011629
2	1.4623	2.1383	0.0016612	0.0011360
3	1.4967	2.2400	0.0016894	0.0011287
4	1.5300	2.3409	0.0017550	0.0011471
5	1.5528	2.4113	0.0017460	0.0011244
6	1.5723	2.4722	0.0017737	0.0011281
7	1.5901	2.5283	0.0018078	0.0011369
8	1.6110	2.5954	0.0018242	0.0011323
9	1.6314	2.6616	0.0018271	0.0011199
10	1.6560	2.7423	0.0018740	0.0011317
11	1.6822	2.8299	0.0018622	0.0011070
12	1.7009	2.8931	0.0019019	0.0011182
13	1.7365	3.0155	0.0019595	0.0011284
14	1.7670	3.1222	0.0019880	0.0011251
15	1.7987	3.2353	0.0019979	0.0011107
16	1.8336	3.3619	0.0020660	0.0011267
17	1.8727	3.5070	0.0021031	0.0011230
18	1.9147	3.6660	0.0021901	0.0011229
19	1.9679	3.8727	0.0021921	0.0011139
20	2.0388	4.1566	0.0022858	0.0011212
21	2.1181	4.4865	0.0023759	0.0011217
22	2.1907	4.7992	0.0024507	0.0011187
23	2.2617	5.1152	0.0025533	0.0011289
24	2.3306	5.4315	0.0025994	0.0011154
25	2.3815	5.6715	0.0026805	0.0011256
26	2.4856	6.1781	0.0027988	0.0011260
27	2.5851	6.6829	0.0029107	0.0011260
28	2.6610	7.0811	0.0030123	0.0011320
29	2.7467	7.5444	0.0031092	0.0011320
30	2.8423	8.0786	0.0032523	0.0011442
31	2.9659	8.7967	0.0033915	0.0011435
32	3.0330	9.1989	0.0034512	0.0011379
33	3.1087	9.6643	0.0035805	0.0011517
34	3.1944	10.2041	0.0036548	0.0011441
36	3.2913	10.8329	0.0037786	0.0011480
37	3.3394	11.1514	0.0038439	0.0011511
38	3.3985	11.5495	0.0039257	0.0011551
39	3.4546	11.9341	0.0039825	0.0011528
40	3.5190	12.3834	0.0040890	0.0011620
41	3.5874	12.8692	0.0041652	0.0011611
42	3.6641	13.4260	0.0042471	0.0011591
43	3.7384	13.9757	0.0043442	0.0011621
44	3.7868	14.3399	0.0044144	0.0011657
45	3.8815	15.0663	0.0045334	0.0011679
46	3.9815	15.8523	0.0046816	0.0011758
47	4.0917	16.7420	0.0048585	0.0011874

Least Square Fit of Points from No. 19 to No. 47

$\gamma = 0.0010968688$ cal./mole-deg^2
$\beta = 0.0000049371$ cal./mole-deg^2
$\theta = 454.741$°K

$C_v = 10.969T + 0.0494T^3$ (cal./mole-deg) X 10^{-4}

A-6 25 at.% Ru-Rh

Weight of Alloy: 29.7761 gm No. of Mole: 0.2907

Weight of Heater-Thermometer Assembly: 5.2538 No. of Mole: 0.0827

Resistance of Heater at 4.2°K: 256.20 ohm

Thermometer calibration parameters: A = -1.012825
B = 0.632941

No. of Point	T (°K)	T^2 ($°K^2$)	C_v (cal/mole-deg)	C_v/T (cal/mole-deg^2)
1	1.4539	2.1138	0.0015968	0.0010983
2	1.4838	2.2017	0.0016207	0.0010923
3	1.5443	2.3850	0.0016995	0.0011005
4	1.6219	2.6304	0.0017851	0.0011006
5	1.6876	2.8481	0.0018451	0.0010933
6	1.7794	3.1664	0.0019572	0.0010999
7	1.8626	3.4694	0.0020327	0.0010913
8	1.9371	3.7527	0.0021138	0.0010912
9	2.0319	4.1286	0.0022266	0.0010958
10	2.1504	4.6631	0.0023727	0.0010988
12	1.9461	3.7873	0.0021225	0.0010906
13	2.0334	4.1346	0.0022137	0.0010887
14	2.1503	4.6237	0.0023490	0.0010924
15	2.2705	5.1552	0.0024815	0.0010929
16	2.3626	5.5818	0.0025975	0.0010994
17	2.4845	6.1729	0.0027216	0.0010954
19	2.6235	6.8829	0.0028952	0.0011036
20	2.7233	7.4162	0.0030019	0.0011023
21	2.8434	8.0848	0.0031683	0.0011143
23	2.5888	6.7021	0.0028361	0.0010955
24	2.7848	7.7550	0.0030709	0.0011027
25	2.9026	8.4249	0.0032029	0.0011035
26	2.9928	8.9567	0.0033357	0.0011146
27	3.1150	9.7035	0.0034678	0.0011132
28	3.2250	10.4005	0.0036351	0.0011272
29	3.3230	11.0421	0.0037293	0.0011223
30	3.4315	11.7752	0.0038711	0.0011281
31	3.5432	12.5544	0.0039927	0.0011269
32	3.6075	13.0139	0.0041546	0.0011517
33	3.6882	13.6028	0.0041947	0.0011373
34	3.7737	14.2410	0.0043426	0.0011507
35	3.8629	14.9220	0.0045164	0.0011692
36	3.9655	15.7248	0.0046437	0.0011710
37	4.0762	16.6153	0.0047832	0.0011735
38	4.1957	17.6035	0.0049686	0.0011842
39	4.3158	18.6260	0.0051341	0.0011896

Least Square Fit of Points from No. 15 to No. 39

γ = 0.0010480844 cal./mole-deg^2
β = 0.0000074244 cal./mole-deg^2
θ = 396.925°K

$C_v = 10.481T + 0.0742T^3$ (cal./mole-deg) X 10^{-4}

A-7 35 at.% Ru-Rh

Weight of Alloy: 29.5421 gm No. of Mole: 0.2889

Weight of Heater-Thermometer Assembly: 5.2476 No. of Mole: 0.0826

Resistance of Heater at 4.2°K: 256.22 ohm

Thermometer calibration parameters: A = -1.020427
B = 0.635107

No. of Point	T (K)	T^2 (K^2)	C_v (cal/mole-deg)	C_v/T (cal/mole-deg^2)
2	1.3558	1.8382	0.0014789	0.0010908
3	1.4092	1.9858	0.0015234	0.0010810
4	1.4827	2.1985	0.0016057	0.0010829
5	1.5630	2.4430	0.0016820	0.0010761
6	1.6651	2.7725	0.0017962	0.0010787
7	1.7485	3.0573	0.0018724	0.0010708
8	1.8043	3.2555	0.0019251	0.0010670
9	1.8692	3.4939	0.0020039	0.0010720
10	1.9383	3.7570	0.0020800	0.0010731
11	2.0317	4.1279	0.0021919	0.0010788
12	2.0719	4.2929	0.0021965	0.0010601
13	2.1227	4.5057	0.0022806	0.0010744
14	2.1984	4.8330	0.0023540	0.0010708
15	2.2908	5.2478	0.0024494	0.0010692
16	2.3016	5.2975	0.0024564	0.0010673
17	2.3393	5.4721	0.0025084	0.0010723
18	2.3861	5.6935	0.0025578	0.0010720
19	2.4395	5.9511	0.0026080	0.0010691
20	2.4924	6.2122	0.0026848	0.0010772
21	2.5544	6.5252	0.0027286	0.0010682
22	2.6272	6.9019	0.0028297	0.0010771
23	2.6461	7.0017	0.0028608	0.0010812
24	2.6870	7.2197	0.0028926	0.0010765
25	2.7295	7.4502	0.0029619	0.0010851
26	2.7762	7.7075	0.0029804	0.0010735
27	2.8263	7.9881	0.0030719	0.0010869
28	2.8819	8.3051	0.0031279	0.0010854
29	2.9419	8.6548	0.0031796	0.0010808
30	3.0067	9.0405	0.0032307	0.0010745
31	3.0759	9.4614	0.0033556	0.0010909
32	3.1577	9.9713	0.0034462	0.0010913
33	3.2398	10.4961	0.0035536	0.0010969
34	3.3689	11.3496	0.0036836	0.0010934
35	3.4637	11.9971	0.0038193	0.0011027
36	3.5629	12.6941	0.0039386	0.0011055
37	3.6495	13.3191	0.0040295	0.0011041
38	3.7439	14.0171	0.0041852	0.0011179
39	3.8516	14.8344	0.0043015	0.0011168
40	3.9658	15.7274	0.0045046	0.0011359

Least Square Fit of Points from No. 14 to No. 40

γ = 0.0010398129 cal./mole-deg^2
β = 0.0000052946 cal./mole-deg^2
θ = 444.269°K

$C_v = 10.398T + 0.0529T^3$ (cal./mole-deg) X 10^{-4}

A-8 40 at.% Ru-Rh

Weight of Alloy: 31.1085 gm No. of Mole: 0.3045

Weight of Heater-Thermometer Assembly: 5.2824 No. of Mole: 0.0831

Resistance of Heater at 4.2 °K: 297.32 ohm

Thermometer calibration parameters: A = -1.018204
B = 0.627112

No. of Point	T (K)	T^2 (K^2)	C_v (cal/mole-deg)	C_v/T (cal/mole-deg^2)
1	1.3971	1.9519	0.0016396	0.0011736
2	1.4635	2.1418	0.0016962	0.0011591
3	1.5427	2.3800	0.0017692	0.0011468
4	1.6024	2.5678	0.0018217	0.0011368
5	1.6540	2.7357	0.0018554	0.0011217
6	1.7150	2.9414	0.0019451	0.0011342
7	1.7956	3.2241	0.0020337	0.0011326
8	1.8461	3.4082	0.0020863	0.0011301
9	1.8747	3.5143	0.0021069	0.0011239
10	1.9403	3.7648	0.0021738	0.0011203
11	2.0187	4.0750	0.0022632	0.0011212
12	2.1240	4.5112	0.0023894	0.0011250
13	2.1480	4.6141	0.0024013	0.0011179
14	2.2167	4.9138	0.0024871	0.0011220
15	2.2986	5.3836	0.0025552	0.0011116
16	2.3884	5.7045	0.0026602	0.0011138
17	2.4957	6.2287	0.0027692	0.0011096
18	2.6337	6.9366	0.0029390	0.0011159
19	2.7461	7.5409	0.0030639	0.0011158
20	2.8250	7.9807	0.0031277	0.0011072
21	2.9123	8.4814	0.0032603	0.0011195
22	2.9862	8.9172	0.0033384	0.0011179
23	3.0712	9.4321	0.0034441	0.0011214
24	3.1384	9.8497	0.0035204	0.0011217
25	3.2195	10.3652	0.0036273	0.0011267
26	3.2993	10.8855	0.0037368	0.0011326
27	3.3928	11.5108	0.0037966	0.0011190
28	3.5031	12.2719	0.0039668	0.0011323
29	3.6249	13.1400	0.0041327	0.0011401
30	3.7732	14.2372	0.0043185	0.0011445
31	3.8403	14.7478	0.0043640	0.0011364
32	3.9250	15.4058	0.0044923	0.0011445
33	4.0153	16.1228	0.0046013	0.0011459
34	4.0936	16.7578	0.0047599	0.0011628
35	4.1916	17.5692	0.0048411	0.0011550

Least Square Fit of Points from No. 12 to No. 35

γ = 0.0010954537 cal./mole-deg^2
β = 0.0000031560 cal./mole-deg^2
Θ = 527.882 °K

$C_v = 10.955T + 0.0316T^3$ (cal./mole-deg) $\times 10^{-4}$

A-9 7 at.% Pd-Rh

Weight of Alloy: 30.6927 gm No. of Mole: 0.2976

Weight of Heater-Thermometer Assembly: 4.9179 No. of Mole: 0.0774

Resistance of Heater at 4.2°K: 297.22 ohm

Thermometer calibration parameters: A = -1.008480
B = 0.624752

No. of Point	T (K)	T^2 (K^2)	C_v (cal/mole-deg)	C_v/T (cal/mole-deg^2)
1	1.3720	1.8825	0.0018150	0.0013229
2	1.3909	1.9346	0.0017858	0.0012839
3	1.4406	2.0753	0.0018621	0.0012926
4	1.4925	2.2276	0.0019443	0.0013027
5	1.5411	2.3751	0.0019853	0.0012882
6	1.5799	2.4962	0.0020119	0.0012734
7	1.6271	2.6475	0.0020750	0.0012753
8	1.6837	2.8349	0.0021416	0.0012719
9	1.7380	3.0208	0.0021795	0.0012540
10	1.7786	3.1633	0.0022287	0.0012531
11	1.8218	3.3189	0.0022746	0.0012486
12	1.8749	3.5154	0.0023504	0.0012536
13	1.9388	3.7588	0.0024343	0.0012556
14	1.9388	3.7588	0.0024160	0.0012461
15	2.0085	4.0340	0.0025081	0.0012488
16	2.1128	4.4639	0.0026589	0.0012585
17	2.2090	4.8799	0.0027385	0.0012397
18	2.2977	5.2794	0.0028426	0.0012372
19	2.3827	5.6773	0.0029323	0.0012307
20	2.4765	6.1330	0.0030604	0.0012358
21	2.5107	6.3034	0.0030974	0.0012337
22	2.5695	6.6023	0.0031634	0.0012311
23	2.6219	6.8743	0.0032387	0.0012353
24	2.6971	7.2744	0.0033326	0.0012356
25	2.7736	7.6928	0.0034443	0.0012418
26	2.8576	8.1659	0.0035414	0.0012393
27	2.9754	8.8530	0.0036677	0.0012327
28	3.0297	9.1791	0.0037468	0.0012367
29	3.1300	9.7968	0.0039254	0.0012541
30	3.2066	10.2826	0.0040088	0.0012501
31	3.2919	10.8369	0.0041053	0.0012471
32	3.3812	11.4327	0.0042480	0.0012563
33	3.4797	12.1083	0.0043518	0.0012506
34	3.6213	13.1137	0.0045887	0.0012671
35	3.6805	13.5461	0.0046689	0.0012686
36	3.7729	14.2345	0.0047990	0.0012720
37	3.8700	14.9773	0.0049556	0.0012805
38	3.9553	15.6443	0.0050612	0.0012796
39	4.0522	16.4205	0.0052225	0.0012888
40	4.1410	17.1478	0.0053813	0.0012995

Least Square Fit of Points from No. 17 to No. 40

γ = 0.0012010038 cal./mole-deg^2
β = 0.0000050313 cal./mole-deg^2
Θ = 451.885°K

$C_v = 12.010T + 0.0503T^3$ (cal./mole-deg) X 10^{-4}

A-10 15 at.% Pd-Rh

Weight of Alloy: 30.3602 gm No. of Mole: 0.2935

Weight of Heater-Thermometer Assembly: 5.2507 No. of Mole: 0.0826

Resistance of Heater at 4.2°K: 296.955 ohms

Thermometer calibration parameters: A = -1.017232
B = 0.627298

No. of Point	T (°K)	T^2 ($°K^2$)	C_v (cal/mole-deg)	C_v/T (cal/mole-deg^2)
1	1.3747	1.8898	0.0018776	0.0013659
2	1.4132	1.9972	0.0019079	0.0013500
3	1.4733	2.1707	0.0019912	0.0013515
4	1.5389	2.3681	0.0020679	0.0013438
5	1.5969	2.5499	0.0021179	0.0013263
6	1.6802	2.8231	0.0022338	0.0013295
7	1.7495	3.0607	0.0023296	0.0013316
8	1.8405	3.3874	0.0024366	0.0013239
9	1.8714	3.5022	0.0024736	0.0013218
10	1.9349	3.7440	0.0025551	0.0013205
11	2.0119	4.0478	0.0026481	0.0013162
12	2.1135	4.4668	0.0027923	0.0013212
13	2.1489	4.6178	0.0028208	0.0013127
14	2.2089	4.8791	0.0028825	0.0013050
15	2.2926	5.2561	0.0030072	0.0013117
16	2.3724	5.6283	0.0030985	0.0013061
17	2.4663	6.0824	0.0032285	0.0013091
18	2.5342	6.4222	0.0033098	0.0013060
19	2.5908	6.7124	0.0034055	0.0013145
20	2.6582	7.0662	0.0034925	0.0013139
21	2.7327	7.4679	0.0035918	0.0013143
22	2.8172	7.9365	0.0037133	0.0013181
23	2.9108	8.4727	0.0038291	0.0013155
24	3.0236	9.1419	0.0040079	0.0013256
25	3.1649	10.0163	0.0042243	0.0013348
26	3.2882	10.8120	0.0043935	0.0013362
27	3.6104	13.0353	0.0048480	0.0013428
28	3.7476	14.0444	0.0050533	0.0013484
29	3.8741	15.0086	0.0052257	0.0013489
30	3.9674	15.7405	0.0054092	0.0013634
31	4.0565	16.4550	0.0055244	0.0013619
32	4.1659	17.3548	0.0057137	0.0013715
33	3.3039	10.9160	0.0043930	0.0013296
34	3.3820	11.4377	0.0044922	0.0013283
35	3.4927	12.1988	0.0046509	0.0013316
36	3.6017	12.9723	0.0048312	0.0013414
37	3.7391	13.9808	0.0050244	0.0013437
38	3.8385	14.7345	0.0051982	0.0013542
39	3.9331	15.4692	0.0053991	0.0013727
40	4.0164	16.1315	0.0055054	0.0013707
41	4.1163	16.9440	0.0056061	0.0013619
42	4.2230	17.8928	0.0058270	0.0013776

Least Square Fit of Points from No. 12 to No. 42

γ = 0.0012806352 cal./mole-deg^2
β = 0.0000049907 cal./mole-deg^2
θ = 453.108°K

$C_v = 12.806T + 0.00499T^3$ (cal./mole-deg) X 10^{-4}

A-11 22 at.% Pd-Rh

Weight of Alloy: 25.9461 gm No. of Mole: 0.2503

Weight of Heater-Thermometer Assembly: 5.2675 No. of Mole: 0.0829

Resistance of Heater at 4.2°K: 297.355 ohm

Thermometer calibration Parameters: A = -1.015841
B = 0.623333

No. of Point	T (°K)	T^2 ($°K^2$)	C_v (cal/mole-deg)	C_v/T (cal/mole-deg^2)
1	1.3344	1.7807	0.0022663	0.0016984
2	1.3719	1.8821	0.0022299	0.0016254
3	1.4182	2.0112	0.0022462	0.0015839
4	1.5094	2.2784	0.0023292	0.0015431
5	1.5849	2.5120	0.0024139	0.0015230
6	1.6545	2.7375	0.0024642	0.0014894
7	1.7145	2.9395	0.0024888	0.0014516
8	1.7929	3.2146	0.0026610	0.0014842
9	1.9078	3.6397	0.0028224	0.0014794
10	1.9394	3.7612	0.0028025	0.0014450
11	2.0201	4.0810	0.0029106	0.0014408
12	2.1136	4.4672	0.0031400	0.0014857
13	2.1221	4.5032	0.0030839	0.0014532
14	2.2437	5.0340	0.0032148	0.0014328
15	2.3279	5.4193	0.0033208	0.0014265
16	2.4247	5.8792	0.0034548	0.0014248
17	2.5219	6.3601	0.0035956	0.0014257
18	2.6542	7.0449	0.0037862	0.0014265
19	2.8032	7.8578	0.0039971	0.0014259
20	2.9224	8.5405	0.0041707	0.0014271
21	3.0381	9.2298	0.0043550	0.0014335
22	3.1727	10.0658	0.0045543	0.0014355
23	3.3528	11.2414	0.0048239	0.0014387
24	3.3939	11.5188	0.0048717	0.0014354
25	3.5035	12.2746	0.0050837	0.0014510
26	3.6240	13.1331	0.0052511	0.0014490
27	3.7660	14.1829	0.0054690	0.0014522
28	3.8252	14.6320	0.0055848	0.0014600
29	3.8859	15.1004	0.0056329	0.0014496
30	3.9572	15.6594	0.0057577	0.0014550
31	4.0330	16.2650	0.0059058	0.0014644
32	4.1154	16.9366	0.0060251	0.0014640
33	4.2097	17.7212	0.0061666	0.0014649

Least Square Fit of Points from No. 16 to No. 33

γ = 0.0013990152 cal./mole-deg^2
β = 0.0000037496 cal./mole-deg^2
θ = 498.414°K

$C_v = 13.990T + 0.0375T^3$ (cal./mole-deg) X 10^{-4}

A-12 30at.% Pd-Rh

Weight of Alloy: 27.4185 gm No. of Mole: 0.2638

Weight of Heater-Thermometer Assembly: 5.2331 No. of Mole: 0.0824

Resistance of Heater at 4.2°K: 296.98 ohm

Thermometer calibration parameters: A = -1.020067
B = 0.628324

No. of Point	T (K)	T^2 (K^2)	C_v (cal/mole-deg)	Cv/T (cal/mole-deg^2)
1	1.4616	2.1362	0.0022670	0.0015510
2	1.5189	2.3071	0.0023578	0.0015523
3	1.5769	2.4866	0.0024295	0.0015407
4	1.6198	2.6237	0.0024917	0.0015383
5	1.6747	2.8048	0.0025353	0.0015128
6	1.7502	3.0631	0.0026210	0.0014975
7	1.8396	3.3841	0.0027495	0.0014946
8	1.8698	3.4961	0.0027839	0.0014889
9	1.9310	3.7288	0.0028684	0.0014854
10	2.0117	4.0468	0.0029809	0.0014818
11	2.1049	4.4304	0.0031114	0.0014782
12	2.2008	4.8436	0.0032395	0.0014719
13	2.2765	5.1826	0.0033161	0.0014567
14	2.3645	5.5911	0.0034524	0.0014601
15	2.4743	6.1221	0.0036007	0.0014552
16	2.5300	6.4007	0.0036754	0.0014528
17	2.5915	6.7159	0.0037709	0.0014551
18	2.6579	7.0642	0.0038590	0.0014519
19	2.7321	7.4643	0.0039705	0.0014533
20	2.8167	7.9340	0.0041085	0.0014586
21	2.9104	8.4706	0.0042686	0.0014667
22	3.0249	9.1502	0.0044460	0.0014698
23	3.1603	9.9876	0.0046554	0.0014731
24	3.2035	10.2622	0.0046967	0.0014661
25	3.2855	10.7944	0.0048002	0.0014610
26	3.3843	11.5432	0.0049377	0.0014590
27	3.4839	12.1377	0.0051506	0.0014784
28	3.6094	13.0281	0.0053235	0.0014749
29	3.6661	13.4401	0.0054672	0.0014913
30	3.7440	14.0176	0.0055504	0.0014825
31	3.8230	14.6153	0.0057513	0.0015044
32	3.9006	15.2148	0.0057903	0.0014844
33	3.9961	15.9685	0.0060034	0.0015023
34	4.0686	16.5532	0.0061261	0.0015057
35	4.1456	17.1864	0.0062301	0.0015028
36	4.2482	18.0471	0.0064434	0.0015167
37	4.3937	19.3049	0.0066937	0.0015235

Least Square Fit of Points from No. 15 to No. 37

γ = 0.0014166872 cal./mole-deg^2
β = 0.0000051808 cal./mole-deg^2
θ = 447.498°K

$C_v = 14.167T + 0.0518T^3$ (cal./mole-deg) X 10^{-4}

A-13 40 at.% Pd-Rh

Weight of Alloy: 31.1681 gm No. of Mole: 0.2988

Weight of Heater-Thermometer Assembly: 5.2831 No. of Mole: 0.0831

Resistance of Heater at 4.2°K: 297.13 ohm

Thermometer calibraion parameters: A = -1.017229
B = 0.627111

No. of Point	T (K)	T^2 (K^2)	C_v (cal/mole-deg)	C_v/T (cal/mole-deg^2)
1	1.4058	1.9762	0.0022808	0.0016225
2	1.4380	2.0678	0.0023432	0.0016295
3	1.4751	2.1760	0.0023657	0.0016037
4	1.5270	2.3317	0.0024229	0.0015867
5	1.5797	2.4955	0.0025081	0.0015877
6	1.6529	2.7320	0.0026163	0.0015829
7	1.7101	2.9243	0.0027062	0.0015825
9	1.8769	3.5227	0.0029307	0.0015615
10	1.9353	3.7454	0.0030027	0.0015515
11	2.0127	4.0511	0.0031415	0.0015608
12	2.0490	4.1986	0.0031921	0.0015579
13	2.0990	4.4060	0.0032613	0.0015537
14	2.1339	4.5536	0.0033038	0.0015482
15	2.1799	4.7521	0.0033768	0.0015491
16	2.2556	5.0879	0.0034518	0.0015303
17	2.3331	5.4432	0.0036195	0.0015514
18	2.1121	4.4609	0.0032582	0.0015426
19	2.2110	4.8884	0.0033981	0.0015369
20	2.2902	5.2451	0.0035224	0.0015380
21	2.3737	5.6343	0.0036412	0.0015340
22	2.4659	6.0807	0.0037859	0.0015353
23	2.5429	6.4661	0.0039241	0.0015432
24	2.5972	6.7456	0.0039792	0.0015321
25	2.6596	7.0735	0.0041094	0.0015451
26	2.7270	7.4368	0.0042172	0.0015464
27	2.7758	7.7051	0.0043056	0.0015511
28	2.8477	8.1095	0.0044351	0.0015578
29	2.9188	8.5195	0.0045714	0.0015662
30	3.0045	9.0267	0.0046911	0.0015614
31	3.0677	9.4108	0.0047939	0.0015627
32	3.1382	9.8482	0.0049046	0.0015629
33	3.2083	10.2932	0.0049908	0.0015556
34	3.2940	10.8506	0.0051521	0.0015641
35	3.3860	11.4653	0.0053474	0.0015792
36	3.4914	12.1896	0.0055103	0.0015783
37	3.5856	12.8564	0.0056560	0.0015774
38	3.7186	13.8281	0.0059238	0.0015930
39	3.7980	14.4246	0.0060808	0.0016011
40	3.8810	15.0622	0.0063066	0.0016250
41	3.9591	15.6743	0.0064054	0.0016179
42	4.0653	16.5265	0.0065829	0.0016193
43	4.1449	17.1805	0.0067027	0.0016171
44	4.2284	17.8797	0.0068950	0.0016306

Least Square Fit of Points from No. 18 to No. 44

γ = 0.0014941364 cal./mole-deg^2
β = 0.0000073946 cal./mole-deg^2
θ = 397.456°K

$C_v = 14.941T + 0.0739T^3$ (cal./mole-deg) $X10^{-4}$

A-14 Pure Paladium

Weight of Alloy: 45.2666 gm No. of Mole: 0.4254

Weight of Heater-Thermometer Assembly: 5.3009 No. of Mole: 0.0834

Resistance of Heater at 4.2°K: 296.97 ohm

Thermometer calibraion parameters: A = -1.007676
B = 0.624920

No. of Point	T (°K)	T^2 ($°K^2$)	C_v (cal/mole-deg)	C_v/T (cal/mole-deg^2)
1	1.3388	1.7924	0.0032276	0.0024108
2	1.3684	1.8726	0.0032737	0.0023923
3	1.4057	1.9759	0.0033966	0.0024164
4	1.4492	2.1001	0.0034784	0.0024002
5	1.4916	2.2249	0.0035664	0.0023909
6	1.5402	2.3722	0.0037277	0.0024203
7	1.5758	2.4831	0.0037602	0.0023862
8	1.6273	2.6482	0.0039035	0.0023987
9	1.6814	2.8271	0.0040452	0.0024059
10	1.7525	3.0712	0.0042081	0.0024012
11	1.8243	3.3279	0.0043519	0.0023856
12	1.9373	3.7530	0.0046207	0.0023852
13	2.0119	4.0479	0.0048149	0.0023932
14	2.1008	4.4135	0.0050419	0.0024000
15	2.2361	4.9999	0.0053899	0.0024105
16	2.3176	5.3711	0.0056132	0.0024220
17	2.4109	5.8122	0.0058555	0.0024288
18	2.4928	6.2142	0.0061196	0.0024549
19	2.5563	6.5348	0.0062681	0.0024520
20	2.6188	6.8582	0.0064235	0.0024528
21	2.6886	7.2283	0.0066041	0.0024564
22	2.7644	7.6420	0.0068230	0.0024682
23	2.8440	8.0883	0.0069659	0.0024493
24	2.9536	8.7239	0.0073185	0.0024778
25	3.0072	9.0431	0.0074645	0.0024822
26	3.0551	9.3338	0.0075997	0.0024875
27	3.1183	9.7237	0.0077913	0.0024986
28	3.1882	10.1645	0.0079727	0.0025007
29	3.2781	10.7458	0.0082102	0.0025046
30	3.3629	11.3088	0.0085571	0.0025446
31	3.4803	12.1125	0.0089174	0.0025622
32	3.5954	12.9266	0.0092858	0.0025827
33	3.6558	13.3651	0.0094211	0.0025770
34	3.8722	14.9941	0.0102153	0.0026381
35	3.9555	15.6463	0.0104713	0.0026472
36	4.0302	16.2425	0.0107221	0.0026605
37	4.1099	16.8914	0.0109890	0.0026738
38	4.2144	17.7612	0.0113432	0.0026915

Least Square Fit of Points from No.11 to No.38.

γ = 0.0023005422 cal./mole-deg^2
β = 0.0000215464 cal./mole-deg^2
θ = 278.282 °K

$C_v = 23.005T + 0.2155T^3$ (cal./mole-deg) $\times 10^{-4}$

APPENDIX B

COMPUTER PROGRAMS

APPENDIX B

COMPUTER PROGRAMS

B-1. The Main Program

This program consists of two major parts:

Part A.

To calculate heat capacity, the characteristics of thermometer calibration curve, and the values of γ, β, as well as Debye temperature, θ. The least square fit is carried out by a subroutine "McPals."

Part B.

To plot a C_v/T versus T^2 curve from above calculated data.

The variable assignments are as follows:

R(I) = Resistance of thermometer at each calibration measurement.

P(I) = Measured vapor pressure of liquid helium.

PI(I) = Chart pressure of liquid helium.

T(I) = Temperature of thermometer at each calibration measurement.

SR1(I) = Initial resistance of thermometer.

SR2(I) = Final resistance of thermometer.

PR(I) = Resistance of thermometer at each heat capacity measurement.

FN1 = number of moles of heater and thermometer assembly.

FN2 = Number of moles of alloy

FRH = Resistance of heater at 4.2°K, in ohm.

TM(I) = Heating period (in second).

CIH(I) = Heating current (in ampere)

IC(I) = Sequential number of curves

M = Total number of measurements

N = Maximum power of the polynomial to be fit, in this case N = 1.

LP = Sequential number of heat capacity measurement. Points of measurement with sequential number less than LP will not be included in the least square fit.

ZE = Zero error of the d-c. amplifier.

```
      PROGRAM ESHPLOT
      DIMENSION R(40), P(40), T(80), PI(80), X(40), Y(40),
                              CV2(80),
     1 R1(80), R2(80), T1(80), T2(80), TM(80), CIH(80), RST(80),
     1  TT(80), C(10), TSQ(80), RR(2.80), IC(80), PR(80),
                              SR1(80),
     1 SR2(80), LBL(15), NPC(4), PRM(4,3), XH(101,4),
                              YV(101,4), LB(14,10),
     1  XSQ(80), YSQ(80)
C      SQRTF(LOGF(R)/(T*2.3026))=C(1)+C(2)*LOGF(R)/2.3026+
C     1     C(3)*(LOGF(R)/2.3026)**2
      READ 1001, (LB(MB,1),  MB=4,13)
      READ 99, NCRV
      MLB=1
      NL=0
      DO 5 L=1,NCRV
      DO 5 MB=4.13
    5 LB(MB,L)=LB(MB.1)
   10 READ 100, M, N
      IF (M) 20,20,25
   20 CALL PLOT (20., 0.,=1) $   STOP
   25 READ 1001, (LB(MB,1), MB=1,3)
  500 FORMAT (30x, 3A8)
      READ 200, ZE
  200 FORMAT (8F10.7)
   99 FORMAT (I10)
```

```
  100 FORMAT (2I10)
      READ 200, (R(I), I=1, M)
      READ 200, (PI), I=1,M)
      MM=2*M
      READ 200,(PI(I), I=1,MM)
      READ 200,(T(I), I=1,MM)
      READ 800,LP
  800 FORMAT (I10)
      DO 30 J=1.M
      I=2*J-1
      T(J)=T(I)+(T(I+1)-T(I))/(PI(I+1)-PI(I))*(P(J)-PI(I))
   30 TT(J) = 1.0
      PRINT 1000
 1000 FORMAT (1H1)
      PRINT 500,(LB(MB,1), MB=1,3)
      PRINT 202
      DO 35 I=1,M
      R(I)=R(I)-ZE
      X(I)=LOGF(R(I))/2.3026
   35 Y(I)=SQRTF(XI)/T(I))
      CALL MCPALS(M,N,0.,TT,X,Y,RR,C,LP,IDEG)
      N2=N+2
      DO 40 I=N2,10
   40 C(I)=0.0
      PRINT 201,(R(I),P(I),T(I),X(I),Y(I),RR(1,I),RR(2,I),
                                  I=1,M)
  201 FORMAT (8X,5F15.7,2E20.7/)
  202 FORMAT (18X,*R*, 14X,*P*,14X.*T*,14X,*X*,14X,*Y*,14X,
     1                          *ERRORS*, 12X,*FRAC ERRORS*)
  204 FORMAT(/8X, 5F20.7,15)
      K=N+1      $          L=3
      IF (C(L)) 2031,2030,2031
 2030 PRINT 2029
 2029 FORMAT (14X,*A*,20X,*B*)
      GO TO 2032
 2031 PRINT 203
  203 FORMAT (14X,*A*,20X,*B*,20X,*C*)
 2032 PRINT 300,(C(I),I=1,K)
C     CALIBRATION PROGRAM ENDS
      PRINT 1000
      PRINT 500, (LB(MB,1),MB=1,3)
      READ 100, M,N
      FJ=4.184
      READ 200, FN1
      READ 200,FN2
      READ 200,FRH
      FRH=FRH*0.9868
      READ 600,(IC(I),I=1,M)
  600 FORMAT (8I10)
      READ 200,(PR(I), I=1,M)
```

```
      READ 200,(SR1(I), I=1,M)
      READ 200, (SR2(I), I=1,M)
      READ 200, (TM(I), I=1,M)
      READ 200, (CIH(I), I=1,M)
      READ 800,LP
 1001 FORMAT (3A8)
      PRINT 302
      DO 70 I=1,M
      CIH(I)=CIH(I)*0.9913
      R1(I)=PR(I)-SR1(I)-ZE
      R2(I)=PR(I)-SR2(I)-ZE
      X=LOGF(R1(I))/2.3026
      T1(I)=X/(C(1)+C(2)*X+C(3)*(X**2))**2
      Y=LOGF(R2(I))/2.3026
      T2(I)=Y/(C(1)+C(2)*Y+C(3)*Y**2))**2
      T(I)=0.5*(T1(I)+T2(I))
      DELT=T2(I)-T1(I)
C     CVT=CV1/T(I)
      CVT=0.000181 5/14.5973*T(I)**2+0.00018
      RST(I)=CIH(I)**2*FRH*TM(I)/FN2*DELT*T(I)*FJ)-FN1*
                                  CVT/FN2
      CV2(I)=RST(I)*T(I)
      TSQ(I)=T(I)*T(I)
      XH(I,1)=TSQ(I)      $      YV(I,1)=RST(I)*10.0**4
   70 CONTINUE
C     RST(I)=C(1)+C(2)*T(I)**2+C(3)*T(I)**4
      DO 80 I=1,M
   80 TT(I)=1.0
      MP=M-LP+1
      CALL MCPALS(MP,N,O.,TT,TSQ,RST,RR,C,LP,IDEG)
      LPP=LP-1
      PRINT 301,(R1(I),R2(I),TM(I),CIH(I),T(I),CV2(I),
                                  TSQ(I),RST(I),
     1   IC(I), I=1,LPP)
  301 FORMAT (8X,2F10.2,F9.3,F9.5,4F12.7,32X,I5/)
      PRINT 305,(R1(I),R2(I),TM(I),CIH(I),T(I),CV2(I),TSQ(I),RST(I),
     1  RR(1,I),RR(2,I),IC(I),I=LP,M)
  305 FORMAT (8X,2F10.2,F9.3,F9.5,4F12.7,2E16.7,15/)
  302 FORMAT(12X,*R1*,8X,*R2*,8X,*TM*,8X,*CIH*,9X,*T*,9X,
                                  CV2*,9X,*TSQ*,
     1    9X,*RST*,10X,*ERRORS*,6X,*FRAC ERRORS*,4X,*C-NO*)
      THETA=(234.0*6.0251*1.3803/(4.184*C(2)))**0.3333
      K=N+1     $     L=3
      IF (C(L)) 3031,3030,3031
 3030 PRINT 303
  303  FORMAT (/12X,*GAMMA*,14X,*ALPHA*,14X,*THETA*)
      GO TO 3032
 3031 PRINT 310
  310 FORMAT (/12X,*GAMMA*,14X,*ALPHA*,14X,*BETA*,*THETA*)
 3032 PRINT 300,(C*I),I=1,K),THETA
  300 FORMAT(//4F20.10//)
      PRINT 304
```

```
  304 FORMAT (/,14X,*FN1*,15X,*FN2*,15X,*FRH*,15X,*ZE*)
      PRINT 300, FN1,FN2,FRH,ZE
      PRINT 400
  400 FORMAT (13X,*PO-RD*,14X,*SM-R-1*,14X,*T-RES-1*,14X,*
                              SM-R-2*,14X,
     1  *T-RES-2*,10X,*C-NO*)
      PRINT 204, (PR(I),SR1(I),R1(I),SR2(I),R2(I),IC(I),
                              I=1,M)
      NPC(1)=M    $ NCOPYS=1    $    NCG=1    $  LSQDEG=N    $
                              NL=O    $    MNPC=101
      PRM(1,1)+C(1)*10.0**4    $    PRM(1,2)=C(2)*10.0**5    $
                              PRM(1,3)=THETA
      LN=O
      DO 9 I=1,NCOPYS
      NL=NL + 1
      IF (NL.GT.MLB) NL=MLB
      DO 6 MB=1,13
     6  LBL(MB)=LB(MB,NL)
          NC=NCG
            CALL    GRAPH (YV,XH,NPC,PRM,LBL,MNPC,NCG,NCRV,
                              LN,LSQDEG,LP)
      CALL PLOT (300,X,3)
     9 CONTINUE
      PRINT 1000
      GO TO 10
      END



      SUBROUTINE GRAPH (YV,XH,NPC,PRM,LBL,MNPC,NCG,NCRV,LN,
                              LSQDEG,LP)
      DIMENSION YV(MNPC,NCG),XH(MNPC,NCG),NPC(4),PRM(4,3),
                              LBL(15)
      COMMON/GRA/LSD
      DATA (NCURVE=0)
      LSD=LSQDEG
C     INITIALIZATION
      CALL PLOT (0.,0.,0, 80., 80.)
      CALL PLOT (0.,-13.75,2)
      CALL PLOT (0.,0.,0)
      CALL PLOT (2.,3.,2)
      CALL PLOT (0.,0.,0)
      IUB=(NCRV/NCG)*20+20
      CALL PLOT (IUB,X,3)
C     GRID
      FN=NCG-1 $ YLBT = FN*0.25+11.0
      CALL CHAR (YLBT,0.0,LBL(1),8,0.0,.15,.1)
      CALL CHAR (YLBT,1.25,LBL(2),8,0.0.,15,.1)
      CALL CHAR (YLBT,2.50,LBL(3),8,0.0,.15,.1)
      CALL PLOT (0.,0.,2)
             FLN=10.0
      IF (LN.NE.0) FLN=0.1
```

```
      DO 2 I=2,10,2
      A=I-1
      CALL PLOT (0.0,A,2)
      CALL PLOT (FLN,A,1)
      CALL PLOT (FLN,A+1.,2)
      CALL PLOT (o.,A+1.,1)
    2 CONTINUE
      CALL PLOT (0.,0.,1)
      DO 3 I=2,10,2
      A=I-1
      CALL PLOT (A,0.0,2)
      CALL PLOT (A,FLN,1)
      CALL PLOT (A+1.,FLN,2)
      CALL PLOT (A+1.,0.,1)
    3 CONTINUE
      CALL PLOT (0.,0.,1)
      CALL PLOT (0.,0.,2)
C     SCALE X
      CALL CHAR (-1.0,2.00,LBL(4),8,0.0.,15,.1)
      CALL CHAR (-1.0,3.25,LBL(5),8,0.0,.15,.1)
      CALL CHAR (-1.0,4.50,LBL(6),8,0.0,.15.,1)
      XS=0.0
      XL=20.0
      C=(XL-XS)/10.0
      ENCODE (6,4,IS)XS
    4 FORMAT (F6.2)
      CALL CHAR (-0.25,-0.26,IS,6,0.0,1./8.,1./12.)
      B=XS
      DO 5 I=1,10
      FF=I  $  F=FF-0.26  $  G=B+C
      ENCODE (6.4,JS)G
      CALL CHAR (-0.25,F,JS,6,0.0,1./8.,1./12.)
      B=G
    5 CONTINUE
C     SCALE Y
      CALL CHAR (2.00,-1.5,LBL(7),8,90.,.15,.1)
      CALL CHAR (3.25,-1.5,LBL(8),8,90.,.15,.1)
      CALL CHAR (4.50,-1.5,LBL(9),8,90.,.15,.1)
      YL=20.0
      YS=0.0
      C=(YL-YS)/10.0
      ENCODE (8,7,KS)YS
    7 FORMAT (F8.3)
      CALL CHAR (0.0,-1.10,KS,8,0.0,1./8.,1./12.)
      B=YS
      DO 9 I=1,10
      F=1  $  G=B+C
      ENCODE (8,7,LS)G
      CALL CHAR (F,-1.10,LS,8,0.0,1./8.,1./12.)
      B=G
    9 CONTINUE
```

```
C     PARAMETER LIST
      DO 20 I=1,3
      YLB=FN*0.25+10.25  $  XLB=3*(I-1)  $  LL=I+9
      CALL CHAR (  YLB,XLB,LBL(LL),8,0.0,.15,.1)
      DO 20 NC=1, NCG
      FN1=NCG-NC  $  YP=FN1*0.25+10.25  $  XP=XLB+1.25
      IF (I.NE,3) GO TO 17
      NCURVE=NCURVE+1
      ENCODE (3,100.NCVE)NCURVE
  100 FORMAT (I3)
      CALL CHAR (YP,9.870,NCVE,3,0.,1./8.,1./12.)
      IF (NCG.EQ.1) GO TO 17
      YSY=YP+0.1  $  XSY=9.0
      CALL SYMBOL (NC,YSY,XSY,80.,80.)
   17 NCM1=NC-1
      IF (NC.GT.1.AND.PRM(NC,I).EQ.PRM(NCM1,I)) GO TO 20
      ENCODE (8,15,JP1)PRM(NC,I)
   15 FORMAT (F8.3)
      CALL CHAR (  YP,  XP,JP1,8,0.,.15,.1)
   20 CONTINUE
      CALL PLOT (0.,0.,2,80.,80.)
      CALL CURVE (YV,XH,NPC,MNPC,NCG,XL,XS,YL,YS,LP)
      CALL PLOT (0.,0.,0.80.,80.)
      CALL CHAR (12.5,0.,LBL(13),8,0.,0.5,1./3.)
      CALL PLOT (20.,0.,2)
      END



      SUBROUTINE CURVE (YV,XH,NPC,MNPC,NCG,XL,XS,YL,YS,LP)
      DIMENSION YV(MNPC,NCG),XH(MNPC,NCG),NPC(4)
      COMMON/CRV/Y(101),X(101),NCURVE
      DATA (NCURVE=0)
      SY=100./((YL-YS)/8.)
      SX=100./((XL-XS)/8.)
      CALL PLOT (YS,XS,0,SY,SX)
      DO 25 NC=1,NCG
      NCURVE=NCURVE+1
      K=NPC(NC)
      DO 3 J=1,K
      Y(J)=YV(J,NC)
    3 X(J)=XH(J,NC)
      IF (K.GE.101) GO TO 9
      DO 5 I=1,K
      CALL SYMBOL (NC,Y(I),X(I),SY,SX)
    5 CONTINUE
      K=NPC(NC)-LP+1
      CALL LSTSQ (K,XL,XS,LP)
    9 DO 10 I=1,101
      IF (Y(I).GT.YL-0.005) Y(I)=YL
      IF (Y(I).LT.YS+0.005) Y(I)=YS
```

```
 10 CONTINUE
 15 CALL PLOT (Y(1),X(1),2,SY,SX)
    IF (Y(1).NE.YS.AND.Y(1).NE.YL) CALL SYMBOL (NC,Y(1),
                                X(1),XY,SX)
    NP=K
    IF (K.LT.101)  NP=101
    DO 20 I=2,NP $ J1=1
    I1=I+1 $ IM1=I-1
    YT1=(Y(I)-YS)*(YL-Y(I)) $ YT2=(Y(IM1)-YS)*(YL-Y(IM1))
    IF (YT1.EQ.0.0.AND,YT2.EQ.0.0) J1=2
    CALL PLOT (Y(I),X(I),X(I),J1,SY,SX)
    IF (YT1.EQ.0.0.AND.I.NE.NP) GO TO 17
    IF (YT1.NE.0.0.AND.I.EQ.NP) GO TO 10 $ GO TO 20
 17 IF (Y(IM1).EQ.YL.AND.Y(I1).LT.YL) GO TO 19
    IF (Y(IM1).LT.YL.AND.Y(I1).EQ.YL) GO TO 19
    IF (Y(IM1).GT.YS.AND.Y(I1).EQ.YS) GO TO 19
    IF (Y(IM1).EQ.YS.AND.Y(I1).GT.YS) GO TO 10 $ GO TO 20
 19 CALL SYMBOL (NC,Y(I),X(I),SY,SX)
 20 CONTINUE
 25 CONTINUE
    CALL PLOT (YS,XS,2,SY,SX)
    END



    SUBROUTINE LSTSQ (K,XL,XS,LP)
    DIMENSION W (101), R(2,101),C(10)
    COMMON/CRV/Y(101),X(101),NCURVE
    COMMON/GRA/N
    PRINT 100
100 FORMAT (13H1LSTSQ OUTPUT,//)
    K=K+LP-1
    DO 5 I=1,K
  5 W(I)=1.0
    KP=K-LP+1
    CALL MCPALS (KP,N,0.0,W,X,Y,R,C,LP,IDEG)
    PRINT 105, NCURVE,(I,R(1,I),R(2,I),I=LP,K)
105 FORMAT (4X,*CURVE NO.*,I3,/,42X,5HERROR,15X,10HFRAC ERROR,
                                //,
   A       (38X,I3,X,2(E12.4,8X)))
    IDEG1=IDEG+1
    PRINT 110, IDEG,(C(I),I=1,IDGE1)
110 FORMAT (//,X,*IDEG=*,I2,/,X,*LSTSQ COEF*,/,(X,5
                                (E16.8,X)))
    DO 10 J=1,101
    X(J)=(J-1)*0.01*(XL-XS)+XS $ Y(J)=0.0
    IF (X(J).EQ.0.0) GO TO 9
    DO 8 I=1,IDEG1
    Y(J)=Y(J)+C(I)*X(J)**(I-1)
  8 CONTINUE $ GO TO 10
  9 Y(J)=C(1)
 10 CONTINUE
    END
```

```
      SUBROUTINE SYMBOL (NC,YI,XI,SY,SX)
      R=0.04
      CALL PLOT (YI,XI,2,SY,SX)
      GO TO (1,2,3,4),NC
    1 CALL CIRCLE (R,RI,XI) $ GO TO 5
    2 CALL TRI (R,YI,XI)    $ GO TO 5
    3 CALL SQU (R,YI,XI)    $ GO TO 5
    4 CALL DIA (R,YI,XI)
    5 CALL PLOT (YI,XI,1,SY,SX)
      END



      SUBROUTING CIRCLE (R,YI,XI)
      CALL PLOT (YI,XI,2,100.,100.)
      CALL PLOT (YI,XI+R,2)
      DO 12 I=10,360,10
      A=I*3,1415926536/180.
      X=R*COSF(A)+XI  $ Y=R*SINF(A)+YI
      CALL PLOT (Y,X,1)
   12 CONTINUE
      CALL PLOT (YI,XI,2)
      END



      SUBROUTINE TRI (R,YI,XI)
      CALL PLOT (YI,XI,2,100.,100.)
      CALL PLOT (-(2./3.)*0.866*R+YI,XI+R,2)
      CALL PLOT ((4./3.)*0.866*R+YI,XI,1)
      CALL PLOT (-(2./3.)*0.866*R+YI,XI-R,1)
      CALL PLOT (-(2./3.)*0.866*R+YI,XI+R,1)
      CALL PLOT (YI,XI,2)
      END



      SUBROUTINE SQU (R, YI,XI)
      CALL PLOT (YI,XI,2,100.,100.)
      CALL PLOT YI-R,XI+R,2)
      CALL PLOT (YI+R,XI+R,1)
      CALL PLOT (YI+R,XI-R,1)
      CALL PLOT (YI-R,XI-R,1)
      CALL PLOT (YI-R,XI+R,1)
      CALL PLOT (YI,XI,2)
      END



      SUBROUTINE DIA (R,YI,XI)
      CALL PLOT (YI,XI,2,100.,100.)
      CALL PLOT (YI,XI+R,2)
```

```
      CALL PLOT (YI+R,XI,1)
      CALL PLOT (YI,XI-R,1)
      CALL PLOT (YI-R,XI,1)
      CALL PLOT (YI,XI+R,1)
      CALL PLOT (YI,XI,2)
      END


      SUBROUTINE MCPALS(M,N,EPS,W,X,Y,R,C,LP,IDEG)
         DIMENSION W(M),X(M),Y(M),A(10,10),SUMXSQ(19),
                                 C(10),R(2,M),B(10)
         SUMXSQ(1)=B(1)=0
         NMX=N
         IF((M-N-1).LT.0) NMX=M-1
         NMX1=NMX+1
      MN=M+LP-1
         DO 1 I=LP,MN
            R(2,I)=1.0
            B(1)=B(1)+Y(I)+W(I)
1           SUMXSQ(1)=SUMXSQ(1)+W(I)
         R(1,1)=B(1)
         NMN=1
         IF(EPS.EQ.0) NMN=NMX
         DO 10 NN=NMN,NMX
            N2=2*NN
            N1=NN+1
            N21=N2-1
            IF(EPS.EQ.0) N21=1
            DO 2 J=N21,N2
               J1=J+1
               IF(J1.LE.NMX1) B(J1)=0
               SUMXSQ(J1)=0
         DO 2 I=LP,MN
                  R(2,I)=R(2,I)*X(I)
                  SUM=R(2,I)*W(I)
                  IF(J1.LE.NMX1) R(1,J1)=B(J1)=B(J1)+SUM*Y(I)
2                 SUMXSQ(J1)=SUMXSQ(J1)+SUM
            DO 3 I=1,N1
               J1=I-1
               DO 3 J=1,N1
3                 A(I,J)=SUMXSQ(J1+J)
            CALL GAUSS (N1,A,B,C)
            DO 4 I=1,N1
4              B(I)=R(1,I)
         DO 8 I=LP,MN
               SUM=C(N1)
               DO 5 J=1,NN
5                 SUM=X(I)*SUM+C(N1-J)
               SUM=Y(I)-SUM
               IF((ABSF(SUM).LT.EPS).OR.(NN.EQ.NMX))GO TO 7
```

```
            DO 6 J=1,NMX1
 6             R(1,J)=B(J)
            GO TO 10
 7          R(1,I)=SUM
 8          CONTINUE
         DO 9 I=LP,MN
 9          R(2,I)=R(1,I)/Y(I)
         IDEG=NN
         RETURN
10       CONTINUE
         RETURN
      END



      SUBROUTING GAUSS(M,A,B,C)
         DIMENSION A(10,10),B(M),C(M)
101      FORMAT (//53X,30H***SINGULAR MATRIX IN GAUSS***//)
         DO 6 K=1,M
            C(1)=0
            IMAX=K
            DO 1 I=K,M
               T=ABSF(A(1,K))
            IF(C(1).GE.T) GO TO 1
               C(1)=T
               1MAX=I
 1             CONTINUE
            IF(C(1).NE.0) GO TO 2
               PRINT 101
               RETURN
 2          IF(K.EQ.IMAX) GO TO 4
               J=IMAX
               T=B(K)
               B(K)=B(J)
               B(J)=T
               DO 3 L=1,M
                  T=A(K,L)
                  A(K,L)=A(J,L)
 3                A(J,L)=T
 4          I=K+1
            DO 5 J=I,M
               T=A(J,K)/A(K,K)
               B(J)=B(J)-B(K)*T
               DO 5 L=I,M
 5                A(J,L)=A(J,L)-T*A(K,L)
 6          CONTINUE
         J=M+1
         DO 8 K=1,M
            I=J-K
            T=0
            IMAX=I+1
            DO 7 L=IMAX,M
```

```
7               T=T+A(I,L)*C(L)
8           C(I)=(B(I)-T)/A(I,I)
        RETURN
      END
```

B-2. Program for Fitting Data to Equation: $C_v = BT^{-2} + \gamma T + \beta T^3$ by Least Squares Method

```
      READ 200, S
      SUMA11=0.0
      SUMA12=0.0
      SUMA13=0.0
      SUMA22=0.0
      SUMA23=0.0
      SUMA33=0.0
      SUMC1 =0.0
      SUMC2 =0.0
      SUMC3= 0.0
      DO 123 I=1,M
      SUMA11=SUMA11+(1.0/T(I)**S)**2.0
      SUMA12=SUMA12+T(I)/(T(I)**S)
      SUMA13=SUMA13+(T(I)**3.0)/(T(I)**S)
      SUMA22=SUMA22+T(I)**2.0
      SUMA23=SUMA23+T(I)**4.0
      SUMA33=SUMA33+T(I)**6.0
      SUMC1 =SUMC1+CV2(I)/(T(I)**S)
      SUMC2 =SUMC2+CV2(I)*T(I)
      SUMC3 =SUMC3+CV2(I)*(T(I)**3.0)
123   CONTINUE
      BA1=SUMA22-(SUMA12*SUMA12)/SUMA11
      BA2=SUMA23-(SUMA12*SUMA13)/SUMA11
      BB2=SUMA33-(SUMA13*SUMA13)/SUMA11
      D1=SUMC2-(SUMA12*SUMC1)/SUMA11
      D2=SUMC3-(SUMA13*SUMC1)/SUMA11
      SEW=BB2-(BA2*BA2)/BA1
      DEW=D2-(BA2*D1)/BA1
      BETA=DEW/SEW
      GAMA=D1/BA1-(BA2/BA1)*BETA
      RAT=SUMC1/SUMA11
      BAU=SUMA13/SUMA11
      ALPHA=RAT-BAU*BETA-(SUMA12/SUMA11)*GAMA
```